NTNU – Trondheim
Norwegian University of
Science and Technology

Battery inductive charging for electrical mobility applications

Bergljot Tjønn

Master of Energy and Environmental Engineering
Submission date: July 2015
Supervisor: Elisabetta Tedeschi, ELKRAFT
Co-supervisor: Giuseppe Guidi, SINTEF

Norwegian University of Science and Technology
Department of Electric Power Engineering

Abstract

This report is a master thesis at the Department of Electrical Engineering at the Norwegian University of Science and Technology (NTNU). The purpose of the thesis was to find a control system used for regulating a system for inductive charging of electric ferries.

Systems for inductive power transfer can be utilized in wireless charging of electric mobility applications. Wireless charging of electric mobility applications is especially advantageous for methods of public transportation that make short, but frequent stops, as buses and ferries. In this thesis, a system for inductive charging of electric ferries will be examined, with system design and specifications provided by SINTEF.

The system is described and simplified in order to derive a transfer function that is simplified using dominant pole approximation. The resulting simplification is a second order transfer function of the form $H(s) = \frac{a_0}{s^2+b_1 s+b_0}$ with the terms a_0, b_1 and b_0 varying according to the distance between the sending and receiving coils. Two scenarios for distance between the coils is looked into: A maximum distance, leading to a low coupling coefficient k for the system, and a minimum distance, leading to a high coupling coefficient for the system. For these cases of coupling two methods for controller design are looked into: Haalman's loop shaping technique and experimental tuning by tuning maps. Based on these methods two controllers with constant gains are designed.

The two methods lead to two controllers: One integral-only controller and one PID-controller in series with a filter. The systems' responses with the two controllers is evaluated and compared, and it is concluded that the integral-only controller is the best choice for controlling the system.

Acknowledgements

I would like to thank prof. Elisabetta Tedeschi for guidance through the last year during my work on my specialization project and master thesis.

In the same manner, I would like to thank my co-supervisor Giuseppe Guidi at SINTEF.

I thank all friends and family for support, encouragement and help.

Contents

List of Figures

List of Tables

Chapter 1

Introduction

Electric vehicles (EVs) have in the later years gained popularity due to increased battery range as well as a higher environmental conscience among consumers [1]. Although electric vehicles are taking up a bigger market share, many are still hesitant to use a battery powered vehicle as the range of usage is more limited than what it is for one powered by gasoline or diesel. One way of challenging this problem is by using inductive power transfer (IPT) systems to charge the vehicles. This charging technology is especially advantageous for EVs used for public transportation, as electric buses or ferries. Both of these stop frequently at bus stops or ferry terminals, and wireless charging for these mobility applications lead to increased charging time, as no time is lost to plugging and unplugging cables.

Inductive power transfer is already a well established technology in various applications, as artificial hearts and other biomedical implants [2]-[4]. Systems for inductive power transfer require complex control of the power flow as the electric parameters can, and most often will, vary during charging due to misalignment between the sending and receiving coils. In spite of difficulties regarding the control system, wireless power transfer is preferable for electric vehicle applications over charging through sockets and cables. It is not only an easy solution for the consumer, but also safe, as overheating

of cables is not a problem, and the system therefore represents a smaller fire hazard [5].

The focus of this work is to find a controller that will be used to control a system for inductive power charging application for electric ferries. First, background information on inductive power transfer and challenges connected to controlling these systems are presented. Next, the specific system that will be considered is discussed and simplified. Chapter 4 discusses control systems, and in the next chapter a mathematical model of the considered IPT system is derived and simplified. Following this, these simplifications will be used to design a control system in the next chapter, using the theory on control systems presented in Chapter 4. Two control systems will be found in this chapter. They will be compared based on the systems' response to a step change in the input and their frequency response as well as the complexity of the control systems, and one of them will be proposed as the most suitable controller for the system.

Chapter 2

Background

This chapter will provide the reader with a historical background of IPT systems, from Tesla's discovery of wireless power transfer to the current state-of-the-art, and the challenges faced in the control of inductive power transfer technology used in electric mobility applications today.

2.1 Discovery of IPT

Inductive power transfer is not a new phenomenon — Nikola Tesla performed several experiments on wireless power transmission as early as the 1890's [6]. In the late 19th and early 20th centuries he managed to use wireless power transfer to light up light bulbs completely without the use of wires. His work was based on the work of several scientists, among which André Marie Ampère, Michael Faraday, Joseph Henry and James Clerk Maxwell are the most important. The work of these men laid as a basis for Tesla's work on the rotating magnetic field and wireless power transmission.

Through Faraday's law of electromagnetic induction it is known that the

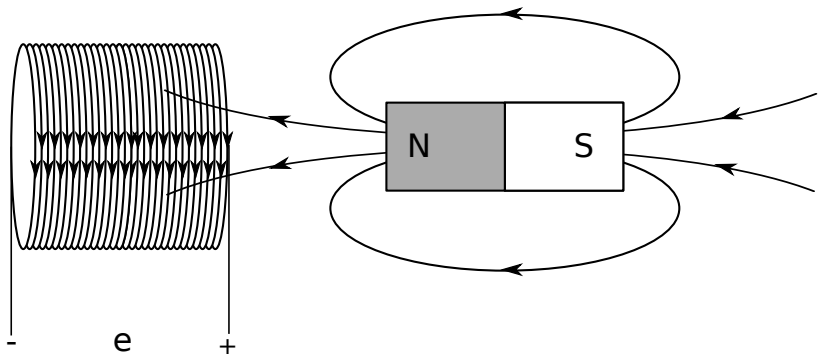

Figure 2.1: The magnet's moving magnetic field induces an emf in the conductor.

total induced electromotive force, emf, is given by the magnetic flux change over a surface S, enclosed by a conductor C with a magnetic field $\mathbf{B}$ acting upon it, as shown in Figure 2.1. In mathematical form Faraday's law is given by:

$$e = \oint_C \mathbf{E}_{ind} \cdot d\mathbf{l} = -\frac{d\Phi}{dt} = -\frac{d}{dt}\int_S \mathbf{B} \cdot d\mathbf{S} \tag{2.1}$$

Faraday's law states that a time-varying magnetic field is always accompanied by a time-varying electric field, and vice versa. This is one of the most important equations describing inductive power transfer. The time-varying magentic field in the sending circuit induces a voltage in the receiving circuit.

2.2 Past and Future Development of IPT

Inductive power transfer laid more or less untouched for several decades, but since the 1960's the technology has been used in biomedical appliances and implants [7]. IPT by inductive coupling of coils was first used to power an artificial heart, and has later been utilized to power implantable devices [3].

General Motors' infamous electric car EV1 used a charging system with inductive, although not wireless, power transfer in the mid 1990's [8]. The system was called the Magne Charge and came in two versions: Level 2 with a capacity of 6.6 kW, and the quicker level 3 with a capacity of 50 kW. In spite of being an inductive charging system, the users still had to connect the charger to the car through a cable. In other words, the Magne Charge prevented the user from experiencing many of the main advantages associated with inductive power transfer when it also is wireless.

When using wireless charging, several charging methods can be used, some more suitable for some mobility applications than others, as the use of vehicles differs. To illustrate these differences, an electric ferry can be compared to a private electric car. An electric ferry follows the same route several times every day, stopping for a certain amount of time at ferry terminals for embarkment and disembarkment of passengers and vehicles. These stops are often short, leading to an increased charging time when no time is lost to plugging and unplugging cables. For a private electric vehicle, on the other hand, if the vehicle is left to charge throughout the night, the time lost to plugging and unplugging the vehicle is negligible when compared to the total charging time.

Similarly to an electric ferry, a public bus will make frequent stops at specific places, giving it the opportunity to have many short recharges if wireless charging stations are put up by each bus stop. Buses can also use other charging strategies, as making longer stops every hour in order to bring the battery to a full recharge. Some buses on the market today can drive for up to 24 hours without the need to conduct a long recharge [9].

Currently, wireless charging of electrical appliances is becoming increasingly available. The technology has been used in charging of electrical toothbrushes for years, and recently several companies have developed wireless charging stations for cellular telephones [10].

In the future, wireless roadway electrification can make dynamic charging a reality, that is charging the vehicle while it is in motion. It works by having the primary side of the IPT system in the road, while the secondary side is in the vehicle. This technology is, however convenient for the user, at the time very expensive as it will require reconstruction of already existing roadways. Another way of using wireless charging is by having charging stations, either public or private, which utilize inductive power transfer for wireless charging of electric vehicles. Roadway electrification will completely eliminate the problems associated with range anxiety for users of electric vehicles, as the battery can be charged while the vehicle is in use.

2.3 Current State-of-the-Art

Dynamic IPT systems give the opportunity to drive constantly without the need of storing big amounts of power in either a fuel tank, as in an internal combustion engine, or a battery [11]. Static charging systems make charging the battery easier and safer for the user, as overheating of wires and sockets is not a problem. Dynamic charging requires a more complex control system, as the coupling coefficient and misalignment will vary during charging.

One of the major challenges in the development of IPT systems, is to have a well functioning control system. The state-of-the-art of control of wireless power transfer for electric mobility applications will be presented in the following. The control of the system can be placed on the primary side, the secondary side or a combination of the two, including control systems which transmit information from the secondary system to the primary system. The control strategies described here are for different systems for inductive

power transfer, and detailed information on each system can be found in the articles that are referred to in each section.

2.3.1 Phase Shift Control

Phase shift control is a control method achieved by varying the switching frequency of the full bridge inverter on the primary side of the IPT system. Varying the switching frequency leads to a variable amplitude of the fundamental output voltage from the inverter [12]. This control method will not be further investigated here, but it will be taken into consideration when simplifying the system.

2.3.2 Power-Frequency Controller

A power–frequency controller for bidirectional inductive power transfer systems can regulate an IPT system based on its power-frequency droop characteristics [13]. The controller is capable of regulating the power flow in both uni- and bidirectional systems with either one or more loads.

The controller is placed on the secondary side of the system. A PI-controller is used to generate the phase shift required to extract the desired power from the primary to the secondary side. The power flow is regulated through controlling the voltage generated by the converter on the pick-up side for a given primary side voltage. Regulation is achieved by driving both legs of the pick-up side converter with respect to each other using a phase shift. A phase shift of 0^o and 360^o correspond to maximum power flow in foreward and reverse direction, respectively, while a phase shift of 180^o corresponds to zero transferred power.

2.3.3 Primary Side Controller

In [14] a primary side controller for use in biomedical devices is presented. The main advantage of this controller, is the elimination of the wireless

feed-back loop needed when having a controller on the primary side that takes the load impedance or output voltage in as an input. The primary side controller the authors propose, utilizes the track voltage to control the output voltage.

The proposed control method uses a PI-controller on the primary side of the system. This PI-controller produces a signal that maintains the required output voltage by controlling the track current. This is achieved by estimating the output voltage and comparing this to a reference voltage that represents the required output voltage. This error signal is passed through the PI-controller which produces the required output voltage. The process of estimating the output voltage from the IPT system happens in four stages: First, the average of the phase difference between the track voltage and the track current is calculated by the controller. Then the track voltage is decompose into real and imaginary parts. The mutual inductance between the pick-up and the track is then found. Lastly, the estimated mutual inductance and the calculated real part of the track voltage are used to predict the output voltage.

The controller is designed for use in biomedical devices and is simulated and tested in a laboratory set-up for a maximum output power of 150 W.

2.3.4 Primary Input Voltage Regulation

In [15] regulation of the primary input voltage is used in a wireless power supply for implantable biomedical devices. The power flow of the system is regulated by controlling the input voltage magnitude of the primary power converter in accordance with the power demands of the load and the dynamic changes of the circuit parameters. The proposed regulator uses radio frequency (RF) digital communication to exchange information between the primary and secondary sides.

2.4 Scope of Work

All the papers presented in the previous section address the same problem: Controlling the power received by the load. The focus of this thesis will be to design a control system for a given system for inductive charging of electric ferries, which keeps the charging current within the limits of constant current, regardless of changes in the coupling between the sending and receiving parts of the system. A mathematical model of the system will be derived and used in the design of the control system and analysis of the resulting system.

Chapter 3

System Theory

This section presents and simplifies a system for inductive power transfer used to charge the battery of an electric ferry. Theory relevant for the control system design is presented and discussed. The purpose of the analysis of this chapter is to later in the thesis establish an appropriate control system for regulating the power flow to the battery during one of its charging regimes.

3.1 Inductive Power Transfer

In a transformer, power is transferred from the transformer's primary coil to the secondary, which are connected by a common core, as shown in Figure 3.1. Inductive power transfer systems transfer energy between two coils without the use of a core or any other physical contact between the primary and secondary. The two coils are *inductively coupled*. The inductive power transfer system that will be described and examined in this thesis, will be a system with loose coupling. In a loosely coupled system, the sending and receiving coils have some distance between each other, leading to some of the flux being lost from the pick-up coil, as shown in Figure 3.2.

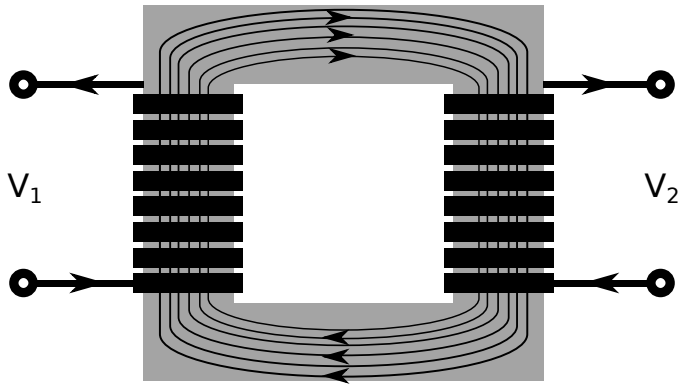

Figure 3.1: Illustration of transformer with flux lines indicated in the core.

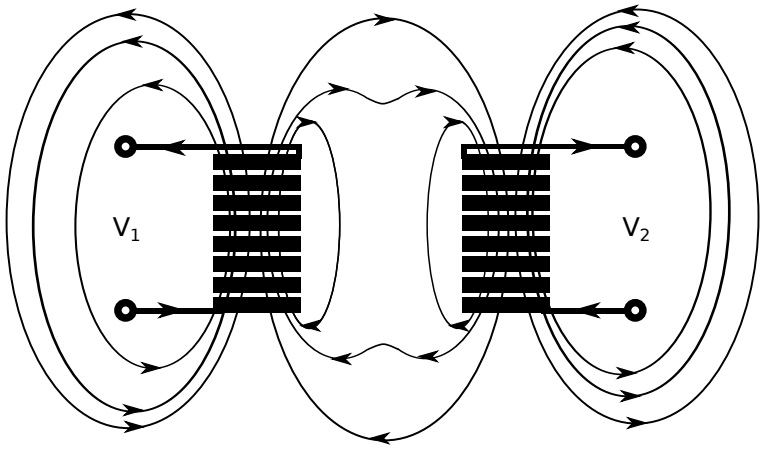

Figure 3.2: Flux lines in system for inductive power transfer.

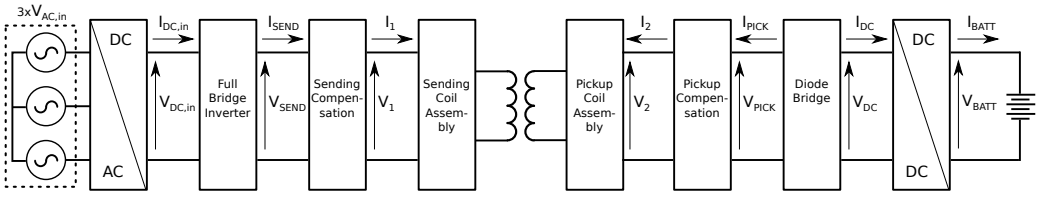

Figure 3.3: Model of the inductive power transfer system.

3.2 IPT System for Electric Mobility Applications

An inductive power transfer (IPT) system consists of two subsystems: The *primary* system and the *secondary* system. The role of the primary system is to wirelessly furnish the secondary system with energy within the required voltage and current constraints of the system's load(s). To achieve the wireless transmission of power, the primary and secondary systems are equipped with coils which allow for inductive power transfer between them. Below is a block diagram showing the unregulated IPT system that will be considered. The system was provided by SINTEF. In the figure, V_2 represents the voltage induced in the secondary circuit due to the primary current i_1 and V_1 is the feedback voltage due to the secondary side current i_2. V_{send} and V_{pick} are the system's sending and receiving (pickup) voltages, respectively.

In Figure 3.3 it is seen that the IPT system is powered by a three phase AC voltage source. A back-to-back AC/AC converter consisting of an AC/DC converter and a full bridge converter (H-bridge) converts the three phase input AC voltage to the single phase AC voltage V_{send}. Capacitive compensation is required as the inductive components of the IPT system produce high amounts of reactive power by transmitter coils [16].

Both the AC/AC converter and the capacitive compensation on the primary side work together to put the primary system into resonance; maximizing the voltage (i.e. the derivative of the magnetic field) across the primary coil. Similarly, the secondary side requires capacitive compensation to put it into

resonance with the primary side's oscillating magnetic field. This ensures maximal coupling between the magnetic field and the secondary pickup coil. This maximization is paramount since the primary and secondary coils will be loosely coupled due to a significant distance separating them.

On the receiving side of the system there is a converter consisting of a diode bridge rectifying the AC voltage to DC, and a DC/DC converter to get the required DC voltage to charge the battery, which is considered to be a lithium-ion type battery. This type of battery is used in most battery electric vehicles today and will be discussed in Chapter 3.6.

In a system for inductive power transfer, the aim is to maximize the transmission distance while minimizing the losses and the effect of misalignment. In addition, the electromagnetic field should be confined in the close proximity of the system.

3.3 Simplified IPT Model

In order to proceed with the coming discussions and analysis, it is necessary to make some simplifications to the IPT model depicted in Figure 3.3. Figure 3.4 reveals these simplifications.

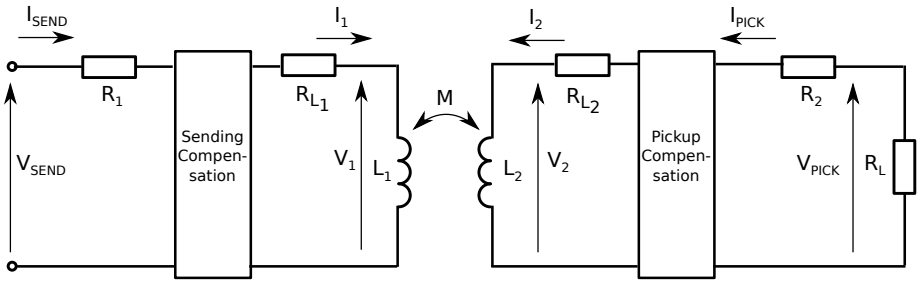

Figure 3.4: Simplified model of the IPT system.

From Figure 3.4 it is evident that the three phase AC to single phase AC

subsystem has been ignored. This is done under the assumption that this part of the IPT system is easily controlled. The coil assemblies have been replaced by an inductor with inductance L_1 and L_2 and with an internal resistance of R_{L_1} and R_{L_2}. The two resistances R_1 and R_2 account for the remaining losses in the system. The AC/DC conversion subsystem on the secondary side represents a non-linear load. It has been lumped together with the battery into a single load, R_L, for convenience in the analysis. The mutual inductance between the two inductors has been represented by a linear non-ideal transformer.

3.4 Coupling Coefficient

The mutual inductance between the two inductors in Figure 3.4 has been represented by a non-ideal linear transformer. In an ideal transformer there are no losses, and the mutual inductance M is given by:

$$M = \sqrt{L_1 L_2} \tag{3.1}$$

However, since the two inductors in the IPT system are loosely coupled due to the distance separating them, this formula must be amended to account for the coupling losses due to this separation:

$$M = k\sqrt{L_1 L_2}, \quad 0 \leq k \leq 1 \tag{3.2}$$

Here k is denoted as the *coupling coefficient* and is simply a dimensionless non-negative real number which is always between zero and 1. A k of 1 indicates a strong coupling and a physical link between the primary and secondary coils (as is found in a transformer), and a coupling coefficient closer to zero indicates weak coupling and longer distances between the sending and receiving coils.

As evident from Equation 3.2, the coupling coefficient will directly influence the mutual inductance of the system.

3.5 Compensation

The inductive components of the IPT system require that the system has some form of reactive compensation in order to achieve optimal operation. Because the coils used for the inductive power transfer are separated by a significant distance in the IPT system, the coupling coefficient of the mutual inductance between the coils will be reduced. Consequently, capacitive compensation on the primary side to maximize the change in the magnetic field, i.e. the voltage across the primary coil, is essential to compensate for the reduced coupling. Compensation on the secondary side is also important as it ensures that the receiving circuit couples maximally with the primary coil's magnetic field. The compensating capacitor can be placed either in parallel or in series with the coil assemblies, on the primary and/or secondary sides. When compensating on both sides, four compensation scenarios are possible: series-series (SS), series-parallel (SP), parallel-series (PS) or parallel-parallel (PP). Here, the first series/parallel represents the primary side compensation and the second series/parallel represents the secondary side compensation. The different compensation scenarios are depicted in Figure 3.5.

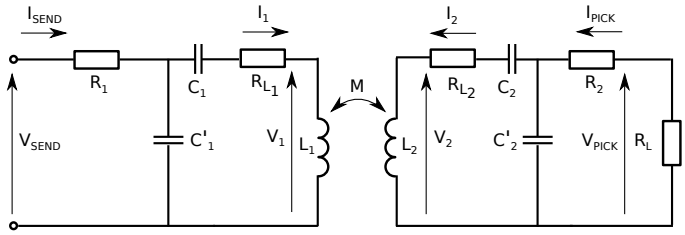

Figure 3.5: Possible capacitive compensation regimes to allow for resonance in the sending and receiving circuits. The capacitor pair selection (C1,C2), (C1,C2'), (C1',C2) and (C1',C1') represent the four possible compensation regimes SS, SP, PS and PP, respectively.

To decide on a compensation scheme to be used in the analysis of this

thesis, the resonant frequency of the system with SS compensation will be derived and discussed.

Determining the resonant frequency as a function of the parameters of the IPT system for each of the four configurations is done by determining the frequency when the imaginary part of the input impedance, Z_{send}, as seen by the voltage V_{send} and current I_{send}, is equal to zero. The input impedance with the SS compensation scenario, $Z_{send,SS}$, is given below. The derivation may be found in Appendix A.1.

$$\text{Re } \{Z_{send,SS}\} = R_{eq1} + \frac{\omega^2 M^2 (R_L + R_{eq2})}{(R_L + R_{eq2})^2 + \left(\omega L_2 - \frac{1}{\omega C_2}\right)^2} \tag{3.3a}$$

$$\text{Im } \{Z_{send,SS}\} = \left(\omega L_1 - \frac{1}{\omega C_1}\right) - \frac{\omega^2 M^2 \left(\omega L_2 - \frac{1}{\omega C_2}\right)}{(R_L + R_{eq2})^2 + \left(\omega L_2 - \frac{1}{\omega C_2}\right)^2} \tag{3.3b}$$

Here $R_{eq1} = R_1 + R_{L_1}$ and $R_{eq2} = R_2 + R_{L_2}$, and the assumption that the load R_L is linear has been made. It is clear from the above equation for Im $\{Z_{send,SS}\}$ that in the SS compensation regime resonance of the system is simply attained when the sending and receiving circuits are tuned to resonate at the same frequency independently of the mutual inductance between them. The condition for resonance along with the resonance frequency in the SS regime is found to be:

$$f_{res,SS} = \frac{\omega_{res,SS}}{2\pi} = \frac{1}{2\pi\sqrt{L_1 C_1}} = \frac{1}{2\pi\sqrt{L_2 C_2}} \tag{3.4}$$

Examining the conditions for resonance in the other three compensation scenarios reveals that all the solutions involve polynomials in ω with coefficients dependent on the mutual inductance M. Such a dependency of the resonance frequency on the mutual inductance is undesirable since the whole system can be put out of resonance if either the primary side or the

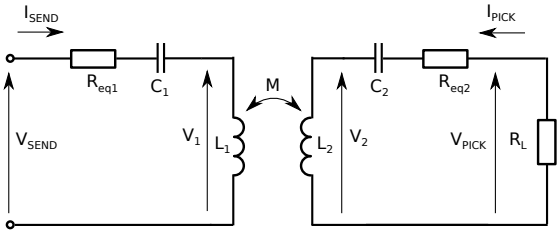

Figure 3.6: Equivalent circuit of simplified IPT system.

secondary side moves relative to the other. *This report will therefore consider a system with SS compensation.* The resulting equivalent circuit of this system is found in Figure 3.6.

3.6 Lithium-ion Batteries

In all electric vehicles used today, batteries are used as a device for energy storage. This is the only way of storing sufficient amounts of energy to give the vehicles a driving range acceptable for the consumer. In a battery, energy is stored as chemical energy and is converted into electrical energy that is used to power the motor of the application. Due to their high energy density, Lithium-ion (Li-ion) batteries are widely used in electric mobility applications. In the following, this type of batteries will be presented.

The Li-ion battery is a rechargeable type of battery. Lithium ions move from a negative to a positive electrode during discharge and back when charging. The positive and negative electrodes are made of lightweight lithium and carbon, respectively. The battery can withstand a high number of charge/discharge cycles and does not have to be completely discharged before charging, which is a necessity in electric mobility applications today.

As stated earlier, lithium ions will move from the positive electrode of the battery to the negative electrode during charging. This happens in two

stages: In constant current (CC) mode and in constant voltage (CV) mode [17]. The charging of the battery is illustrated in Figure 3.7.

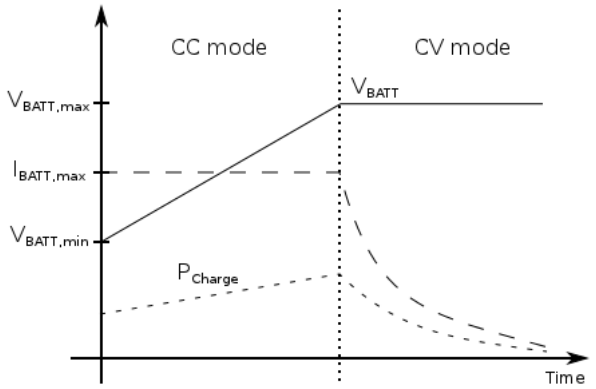

Figure 3.7: CC and CV mode of battery charging.

During CC mode, the current is held at a constant level while the voltage increases. When the voltage level $V_{BATT,max}$ is reached, the charging goes into CV mode, in which the voltage is kept constant while the current decreases. While charging under CC conditions, it is important that the current remains constant. As can be observed by looking at Figure 3.7, the power is higher during charging in CC mode. Because of this, this charging mode is usually used during fast charging. In this thesis, the controller will be designed for charging under the condition of constant current.

Chapter 4

Control Theory

The purpose of a regulator is to keep the output of the system transfer function within specified limits, regardless of what the input into the process is. In addition, a good regulator will make a process that is unstable, stable, and keep an already stable process within the stability margins. In this chapter, theory relevant for the coming design of the system's control system will be presented. Based on this theory, a control system fit for the system will be designed in Chapter 6.

4.1 Control System Representation

To describe a control system, a system is usually represented by its Laplace transform. In the analysis now undertaken, lower case letters will be used to represent functions in the time domain, and capital letters will represent their corresponding Laplace transforms in the s-plane.

A physical system can be described by the system's transfer function $H_u(s)$. Figure 4.1 shows a block diagram of a closed loop control system with a feedback controller. Here, U represents the input signal to the process,

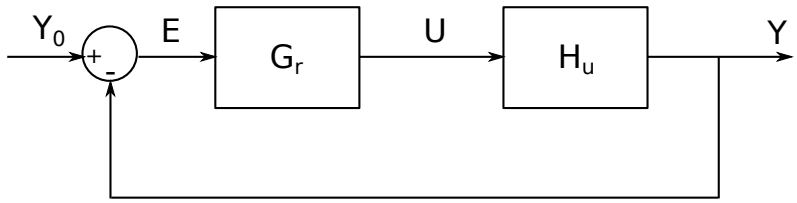

Figure 4.1: Block diagram of feedback control system.

Y represents the output from the system, and $H_u(s) = \frac{Y}{U}$ represents the system transfer function. In the closed loop system, there is a feedback loop with which the reference signal Y_0 creates the error signal $E(s) = Y_0 - Y$ which is taken as an input into the regulator, which in the block diagram is represented by the transfer function $G_r(s)$. The signal U is then received by the system $H_u(s)$, which creates the output signal Y. The system of Figure 4.1 utilizes a unity feedback controller.

The transfer function of a system can often be simplified to a lower order transfer function. Order reduction of transfer function is especially advantageous when the original transfer function consists of a high number of states. In that case, accurate simplified models can be computed and used in the analysis of the system.

In the analysis of the control system, the input signal U will be represented by a step response as it is assumed that the reference signal may change at certain time instances. It is further assumed that the control system does not produce any noise or disturbances to the signals. This will not be the case in a real system, but it is assumed here to simplify the analysis.

4.2 Process of Control System Design

The control system will be designed in the following way:

1. A tuning method will be chosen.
2. The controller will be designed separately for the system with low and high coupling coefficients.
3. A controller that works for both coupling scenarios will be designed based on the results found in the previous step.
4. The controller will be tested and evaluated for both scenarios of coupling coefficient. If necessary, step 3 will be repeated.
5. The controller will be tested and evaluated for the non-simplified systems.

4.3 PID controllers

PID controllers are proportional-integral-derivative controllers, and comprise a proportional, an integral and a derivative term. In the Laplace domain the controller can be represented by the expression

$$H_{PID}(s) = K_p + \frac{K_i}{s} + K_d s = \frac{K_d s^2 + K_p s + K_i}{s} \tag{4.1}$$

Here, K_p, K_i and K_d are the proportional, integral and derivative gains, respectively. The P-term is proportional to the error, the I-term is proportional to the integral of the error and the D-term is proportional to the derivative of the error. The P-, I- and D-terms can be combined to form variations of the PID controller as the PI, PD, P and I controllers. Proportional-only (P) control of a process often leads to a steady state error. In order to eliminate this steady state error, integral control can be added to a control loop. With integral control, a small positive error will always lead to an increasing control signal and a negative error will lead to a decreasing control signal. The purpose of the derivative term is to improve the closed loop stability. [24]

PID controllers are used in 95% of all processes and have proven to be a good controller in many applications [18]. During the 1930's, PID controllers became available, and Ziegler and Nichols proposed their PID tuning rule in 1942 [19]. The main advantage of this tuning rule is that detailed knowledge about the process is not required, as it is an experimental tuning rule. Since the publication of the article introducing the Ziegler-Nichols tuning rule, several tuning rules have been proposed, and used successfully by the industry [20]-[21]. The Ziegler-Nichols tuning rule is based on the ultimate gain of the system (the gain at which the system is marginally stable) and the oscillation time of the system with this ultimate gain. This and similar methods have shown to work well for several process models, but a prerequisite for using the tuning rules that are based on the ultimate gain is that *an ultimate gain exists for the process.* If an ultimate gain does not exist, as will be discussed that is the case for the simplified transfer function found for the considered system in Chapter 5, a different tuning method must be used.

There are several tuning methods that can be used to tune systems without ultimate gain. In the following sections, methods for finding a controller of such processes will be presented.

4.4 Haalman's Loop Shaping Method

The Haalman method for loop shaping is based on determining an ideal loop transfer function G_l and choose the controller transfer function as $G_c = \frac{G_l}{H_u}$ [24]. This method does not necessarily lead to finding a PID controller for tuning the system, but that can be the case if G_l and H_u are sufficiently simple. The main challenge with using this method is finding a suitable ideal loop transfer function.

4.5 Experimental Tuning by Tuning Maps

Manual tuning can be used both when doing corrections to controller parameters to obtain a desired performance or to find the controller parameters from scratch. To guide manual tuning, tuning maps can be used. Tuning maps are two dimensional arrays of transient or frequency responses that show how changes in the controller parameters influence the behaviour of the closed loop system [24]. The maps can guide the designer to choosing the design that gives the wanted response.

4.6 Integral Performance Criteria

A method of designing a controller is using the integral performance criteria [28]. In this method, the designer looks at the integral of the error signal, minimizes this, and in that way finds the values of K_p and K_i of the regulator function

$$H_c = K_p + \frac{K_i}{s} \tag{4.2}$$

There are several forms of the integral performance criteria, as the Integral of Square Error (ISE), Integral of Absolute Error (IAE), Integral of Time Absolute Error (ITAE), to name a few. These performance criteria are given by

$$ISE = \int_0^T e^2(t)dt \tag{4.3}$$

$$IAE = \int_0^T |e(t)|dt \tag{4.4}$$

and

$$ITAE = \int_0^T t \cdot |e(t)| dt \tag{4.5}$$

Here, $e(t)$ is the error signal and it is integrated from $t = 0$ to $t = T$, where T is a time by which the steady state error is negligible.

These methods are usually used to evaluate *how well* a controller regulates a system. Different regulators can be checked, and the one that gives the smallest error integral will be chosen as the optimal controller. The performance criteria can also be used *to find* the controller gains by minimizing the error integral with respect to K_p and K_i. The resulting coefficients will then yield the controller that provides the system with the smallest error. The use of this method will be discussed in the *Further Work* chapter.

Chapter 5

Mathematical Model of System

In this section a mathematical model of the simplified IPT system found in Chapter 3 will be derived. This model will be used when designing the control system for the IPT system. The dynamic equations of the system will be derived and used to find the state-space model of the system. This system will be used to find the transfer function representation of the system that in the end of this chapter will be simplified to a second order transfer function that will be used in the design of the control system.

5.1 System Parameters

Table 5.1 shows the system parameters used for the system for inductive charging of electric ferries examined in this thesis. The system is designed for transfer of 1 MW of power. These parameters were provided by SINTEF and will be used in the derivation of the system transfer function.

As observed from the table, the inductances are given with a *min* or *max*

Rated Power	P_{rat}	$1MW$
Rated Voltage	$V_{dc,in} = V_{dc,out}$	$1kV$
Inductances	$L_{1,min} = L_{2,min}$	$60.6\mu H$
	M_{min}	$11.3\mu H$
	$L_{1,max} = L_{2,max}$	$68.1\mu H$
	M_{max}	$39.4\mu H$
Capacitances	$C_1 = C_2$	$8.7\mu F$
Loss Parameters	$R_1 = R_2$	$5.6m\Omega$
Resonant Frequency	$f_{res,min}$	$6.93kHz$
	$f_{res,max}$	$6.54kHz$

Table 5.1: System parameters for IPT system for electric ferries.

subscript. These subscripts indicate the value of the coupling coefficient: The min subscript indicates a low coupling coefficient and thereby a longer distance between the sending and receiving coils, while the max subscript indicates a high coupling coefficient and a short distance between the two coils.

Transfer functions will be derived for both of these coupling scenarios and denoted by *low* or *high* depending on which coupling scenario it is. The two resulting transfer functions will be referred to as *the transfer functions of the two systems*, meaning the transfer function of the system with low coupling and the transfer function of the system with high coupling.

5.2 System Transfer Functions

The dynamic equations governing the system, will be derived in this section. These equations will be used to find a state-space model describing the system, which in turn will give the transfer functions of the system with low and high coupling coefficients.

To derive the dynamic equations of the system, Kichhoff's voltage law is

used for both of the circuits shown in Figure 3.6 [22]. In differential form KVL gives:

$$-v_{send} + i_{send}R_{eq1} + v_{C1} + L_1\frac{di_{send}}{dt} - M\frac{di_{pick}}{dt} = 0 \tag{5.1}$$

$$-v_{pick} + i_{pick}R_{eq2} + v_{C2} + L_2\frac{di_{pick}}{dt} - M\frac{di_{send}}{dt} = 0 \tag{5.2}$$

In addition, the currents i_{send} and i_{pick} are described by the primary and secondary side capacitances:

$$C_1 \cdot \frac{dv_{C1}}{dt} = i_{send} \tag{5.3}$$

$$C_2 \cdot \frac{dv_{C2}}{dt} = i_{pick} \tag{5.4}$$

Rearranging the equations gives the following set of equations, arranged in a form more suitable for analysis:

$$L_{\sigma1} \cdot \frac{di_{send}}{dt} = -R_{eq1}i_{send} + \frac{MR_{eq2}}{L_2} \cdot i_{pick} - v_{c1} + \frac{M}{L_2} \cdot v_{c2} + v_{send} - \frac{M}{L_2} \cdot v_{pick} \tag{5.5a}$$

$$L_{\sigma2} \cdot \frac{di_{pick}}{dt} = -R_{eq2} \cdot i_{pick} + \frac{MR_{eq1}}{L_1} \cdot i_{send} - v_{c2} + \frac{M}{L_1} \cdot v_{c1} + v_{pick} - \frac{M}{L_1} \cdot v_{send} \tag{5.5b}$$

$$C_1 \cdot \frac{dv_{C1}}{dt} = i_{send} \tag{5.5c}$$

$$C_2 \cdot \frac{dv_{C2}}{dt} = i_{pick} \tag{5.5d}$$

with $L_{\sigma1}$ and $L_{\sigma2}$ defined as $L_{\sigma1} = L_1 - \frac{M^2}{L_2}$ and $L_{\sigma2} = L_2 - \frac{M^2}{L_1}$. As noted, the load R_L is non-linear due to the diode-bridge preceding the

lithium-ion battery (see Figure 3.3). However, by ensuring that the system is not unstable by insisting that R_L is a time independent load, the voltages and currents in the system will eventually go into steady oscillations with the frequency of the source voltage v_{send}. The non-linear load R_L, if time independent, may therefore be linearized around an appropriate current in the steady state region of the system. The linearized system may be expressed by phasors as follows:

$$(x_d(t) + ix_q(t))\, e^{j\omega t} \tag{5.6}$$

Here, x_d and x_q represent the real and imaginary parts, respectively, of a voltage or current in the system, and ω is the frequency of the source voltage v_{send}. The system of equations may now be written as equations of eight unknowns represented by the imaginary and real parts of the voltages and currents:

$$\frac{di_{send,d}}{dt} = -\frac{R_{eq1}}{L_{\sigma_1}} \cdot i_{send,d} + \omega \cdot i_{send,q} + \frac{MR_{eq1}}{L_{\sigma_1} L_2} \cdot i_{pick,d} - \frac{1}{L_{\sigma_1}} \cdot v_{c_1,d} + \frac{M}{L_{\sigma_1} L_2} \cdot v_{c_2,d} + \frac{1}{L_{\sigma_1}} \cdot v_{send,d} - \frac{M}{L_{\sigma_1} L_2} \cdot v_{pick,d} \tag{5.7a}$$

$$\frac{di_{send,q}}{dt} = -\omega \cdot i_{send,d} - \frac{R_{eq1}}{L_{\sigma_1}} \cdot i_{send,q} + \frac{MR_{eq2}}{L_{\sigma_1} L_2} \cdot i_{pick,q} - \frac{1}{L_{\sigma_1}} \cdot v_{c_1,q} + \frac{M}{L_{\sigma_1} L_2} \cdot v_{c_2,q} + \frac{1}{L_{\sigma_1}} \cdot v_{send,q} - \frac{M}{L_{\sigma_1} L_2} \cdot v_{pick,q} \tag{5.7b}$$

$$\frac{di_{pick,d}}{dt} = \frac{MR_{eq1}}{L_{\sigma_2} L_1} \cdot i_{send,d} - \frac{R_{eq2}}{L_{\sigma_2}} \cdot i_{pick,d} + \omega \cdot i_{pick,q} + \frac{M}{L_{\sigma_2} L_1} \cdot v_{c_1,d} - \frac{1}{L_{\sigma_2}} \cdot v_{c_2,d} - \frac{M}{L_{\sigma_2} L_1} \cdot v_{send,d} + \frac{1}{L_{\sigma_2}} \cdot v_{pick,d} \tag{5.7c}$$

$$\frac{di_{pick,1}}{dt} = \frac{MR_{eq1}}{L_{\sigma_2} L_1} \cdot i_{send,d} - \omega \cdot i_{pick,d} - \frac{R_{eq2}}{L_{\sigma_2}} \cdot i_{pick,q} + \frac{M}{L_{\sigma_2} L_1} \cdot v_{c_1,q} - \frac{1}{L_{\sigma_2}} \cdot v_{c_2,q} - \frac{M}{L_{\sigma_2} L_1} \cdot v_{send,q} + \frac{1}{L_{\sigma_2}} \cdot v_{pick,q} \tag{5.7d}$$

$$\frac{dv_{c_1,d}}{dt} = \omega \cdot v_{c_1,q} + \frac{1}{c_1} \cdot i_{send,d} \tag{5.7e}$$

$$\frac{dv_{c_1,q}}{dt} = -\omega \cdot v_{c_1,d} + \frac{1}{c_1} \cdot i_{send,q} \tag{5.7f}$$

$$\frac{dv_{c_2,d}}{dt} = \omega \cdot v_{c_2,q} + \frac{1}{c_2} \cdot i_{pick,d} \tag{5.7g}$$

$$\frac{dv_{c_2,q}}{dt} - \omega \cdot v_{c_2,d} + \frac{1}{c_2} \cdot i_{pick,q} \tag{5.7h}$$

Since the load R_L is assumed to be time independent, it is purely a function of the current i_{pick}. Consequently, the voltage v_{pick} is also purely a function of the current i_{pick}. The above system of equations may therefore be expressed in the following form:

$$\dot{x} = f(x) + h(u) \tag{5.8}$$

where x and u are given by:

$$x = \begin{pmatrix} i_{send,d} \\ i_{send,q} \\ i_{pick,d} \\ i_{pick,q} \\ v_{c1,d} \\ v_{c1,q} \\ v_{c2,d} \\ v_{c2,q} \end{pmatrix} \quad u = \begin{pmatrix} v_{send,d} \\ v_{send,q} \end{pmatrix} \tag{5.9}$$

When Equation 5.8 is linearized around some operating point $x = x_0$ and $u = u_0$, it takes the following matrix form:

$$\dot{x} = f(x_0) + \left.\frac{\partial f}{\partial x}\right|_{x=x_0} (x - x_0) + h(u_0) + \left.\frac{\partial h}{\partial u}\right|_{u=u_0} (u - u_0) \tag{5.10}$$

The equation may be rewritten in the more convenient form:

$$\dot{x} = Ax + Bu + c \tag{5.11}$$

Where A, B and c are as follows:

$$A = \left.\frac{\partial f}{\partial x}\right|_{x=x_0} \tag{5.12a}$$

$$B = \left.\frac{\partial h}{\partial u}\right|_{u=u_0} \tag{5.12b}$$

$$c = \left(f(x_0) - \left.\frac{\partial f}{\partial x}\right|_{x=x_0} x_0\right) - \left(h(u_0) - \left.\frac{\partial h}{\partial u}\right|_{u=u_0} u_0\right) \tag{5.12c}$$

Based on the system of equations found describing the system, the matrix A is found to be:

$$A = \begin{pmatrix} -\frac{R_1}{L_{\sigma 1}} & \omega & \frac{M(R_2+\frac{v_{pick,0}}{v_{send,0}}\cdot\omega M)}{L_{\sigma 1}L_2} & 0 & -\frac{1}{L_{\sigma 1}} & 0 & \frac{M}{L_1 L_2} & 0 \\ -\omega & -\frac{R_1}{L_{\sigma 1}} & 0 & \frac{MR_2}{L_{\sigma 1}L_2} & 0 & -\frac{1}{L_{\sigma 1}} & 0 & \frac{M}{L_{\sigma 1}L_2} \\ \frac{MR_1}{L_{\sigma 2}L_1} & 0 & -\frac{(R_2+\frac{v_{pick,0}}{v_{send,0}}\cdot\omega M)}{L_{\sigma 2}} & \omega & \frac{M}{L_{\sigma 2}L_1} & 0 & -\frac{1}{L_{\sigma 2}} & 0 \\ 0 & \frac{MR_1}{L_{\sigma 2}L_1} & -\omega & -\frac{R_2}{L_{\sigma 2}} & 0 & \frac{M}{L_{\sigma 2}L_1} & 0 & -\frac{1}{L_{\sigma 2}} \\ \frac{1}{C_1} & 0 & 0 & 0 & 0 & -\omega & 0 & 0 \\ 0 & \frac{1}{C_1} & 0 & 0 & -\omega & 0 & 0 & 0 \\ 0 & 0 & \frac{1}{C_1} & 0 & 0 & 0 & 0 & \omega \\ 0 & 0 & 0 & \frac{1}{C_1} & 0 & 0 & -\omega & 0 \end{pmatrix} \tag{5.13}$$

And the matrix B is given by:

$$B = \begin{pmatrix} \frac{1}{L_{\sigma 1}} \\ 0 \\ -\frac{M}{L_{\sigma 2}L_1} \\ 0 \\ 0 \\ 0 \\ 0 \\ 0 \end{pmatrix} \tag{5.14}$$

Since the matrix B is constant, the second term containing h in 5.12c sums to zero. Hence, the vector c is given by:

$$c = f(x_0) - A(x_0)x_0 \tag{5.15}$$

If the load R_L is linear, then the matrix A is also constant: This yields $c = 0$. The equation in 5.11 then takes on the following form for the linear load:

$$\dot{x} = Ax + Bu \tag{5.16}$$

The output vector y is given by $y = Cx + Du$ with C and D given by

$$C = \begin{pmatrix} 0 & 0 & 0 & -\frac{\sqrt{2}}{\pi} & 0 & 0 & 0 & 0 \end{pmatrix} \tag{5.17}$$

and

$$D = 0 \tag{5.18}$$

In case of a time-invariant passive load, the voltage v_{pick} is a function of the current i_{pick}: $v_{pick} = f(i_{pick})$. This function can be expressed in different forms, depending on how one chooses to represent the load. Here, the load is considered to be time-invariant and constant.

The transfer function of this state-space model is defined as $H(s) = \frac{Y(s)}{U(s)}$. To find the system transfer function for the systems with high and low coupling coefficients, MatLab is used. The resulting transfer functions are of the eighth order, and these will be simplified in the next section.

5.3 Order Reduction of System Transfer Function

The dynamic equations represent a system of the eighth order. For the simplicity of the analysis it is advantageous to reduce the order of the system.

Both the model of the system with high and low coupling have four pairs of complex poles. Out of these four pairs, the pole pair placed closest to the imaginary axis is dominant, and this dominant pole pair will be used to find an approximation of the transfer functions. The Bode plot of the full system transfer function and the approximated model will be considered when evaluating how well the approximation works.

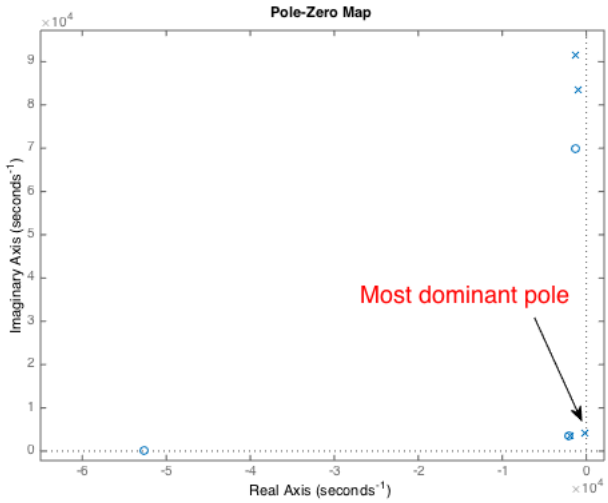

Figure 5.1: Second quadrant of pole-zero map for system with low coupling. The x's denote poles and the o's denote zeros.

In the case of low coupling, the most dominant pole pair is found at $s = (-2.28 \cdot 10^2 \pm j4.07 \cdot 10^3)$, as can be seen in Figure 5.1. The Bode plots of the full system model and the model approximation with only this dominant pole pair is found in Figure 5.2. By comparing the plots, it is obvious that the approximated model has the wrong dc-gain. The appropriate dc-gain is found by finding the ratio of the dc-gain of the full system model to the approximated one. The resulting Bode plots are shown in Figure 5.3.

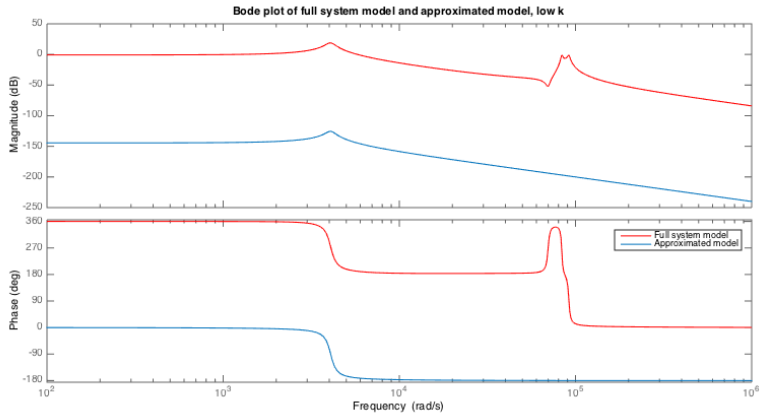

Figure 5.2: Bode plot of full system model and approximated model with low coupling.

Following the same procedure for the system with high coupling, yields the Bode plots depicted in Figure 5.4.

The resulting system transfer functions are of the second order and given as

$$H_{red,highk}(s) = \frac{2.291 \cdot 10^7}{s^2 + 4064s + 8.238 \cdot 10^7} \tag{5.19}$$

and

$$H_{red,lowk}(s) = \frac{1.517 \cdot 10^7}{s^2 + 455.9s + 1.659 \cdot 10^7} \tag{5.20}$$

Figures 5.3 and 5.4 show that the Bode plots of the approximated transfer functions match the Bode plot of the full transfer function well for the low frequencies plotted, but that the approximated and full transfer functions differ for higher frequencies. For both cases of coupling coefficient, the

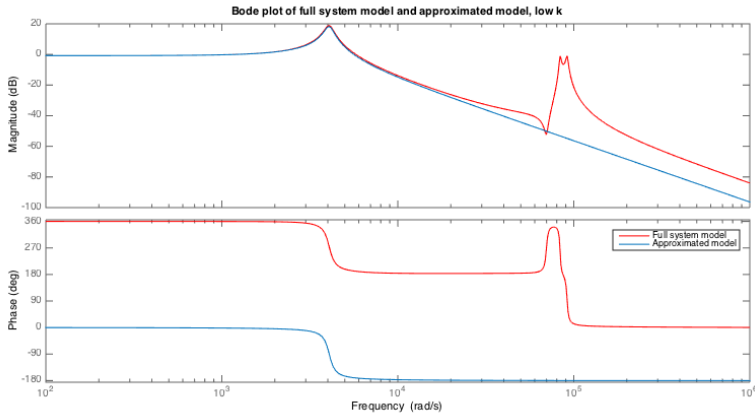

Figure 5.3: Bode plot of full system model and approximated model with low coupling, with matching dc-gain.

simplified transfer functions match the full transfer functions at the first resonant peak in the Bode plot. With this as a requirement, the proposed simplified transfer functions are accepted as the transfer functions that will be used further in the analysis. The simplified transfer function are of the form $H_{red}(s) = \frac{a_0}{s^2+b_1 s+b_0}$ with the constants a_0, b_1 and b_0 given as in Table 5.2. The MatLab code used to find the full system transfer functions and their simplification can be found in Appendix A.2.

The phase vs. frequency plots in the frequency response diagrams show that there is a deviation between the full and approximated models: The full systems begin with a phase shift of 360^o whereas the approximated models begin with a phase shift of 0^o. Since a phase shift of 360^o corresponds to a phase shift of 0^o, this deviation between the full and simplified models does not make a difference for the response of the systems.

In Figure 5.5 a comparison of the full and simplified systems is shown for both coupling cases. As seen from the figure, the simplified transfer function gives a step response very similar to the original transfer function

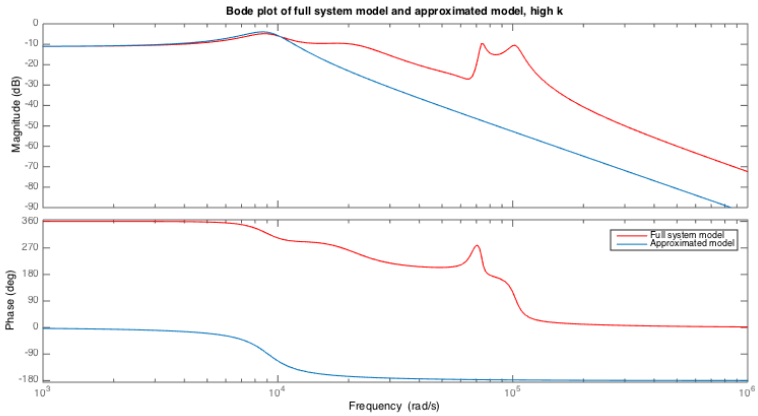

Figure 5.4: Bode plot of full system model and approximated model with high coupling, with matching dc-gain.

	a_0	b_1	b_0
Low k	$1.517 \cdot 10^7$	455.9	$1.659 \cdot 10^7$
High k	$2.291 \cdot 10^7$	4064	$8.238 \cdot 10^7$

Table 5.2: Constants of transfer functions for low and high coupling systems.

in the case of low coupling. For the system with high coupling, however, the simplified transfer function does not give as accurate a response. Examining the step responses for the case of high coupling shows that the overshoot and settling times are very similar for the full and simplified models so the model is considered satisfactory.

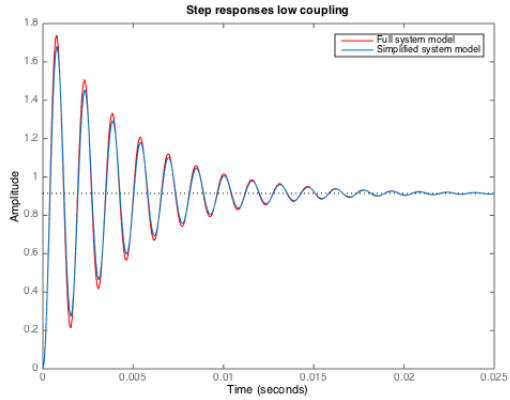

(a) Low coupling

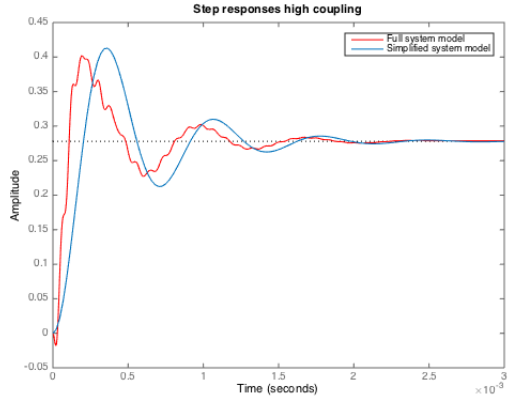

(b) High coupling

Figure 5.5: Plots showing step responses of full and simplified systems.

Chapter 6

Design of Control System

In this chapter a control system which ensures optimal operation of the system described in the preceding chapters will be designed, based on the control system theory of Chapter 4 and using the simplified system transfer functions found in Chapter 5.

6.1 System response

The target of the control system will be to control the power flow into the battery on the receiving side of the IPT system during CC mode of charging, as discussed in Chapters 2 and 3. The control system will therefore regulate the current to have a constant value, regardless of changes in the coupling coefficient k. In addition to regulating the current level on the secondary side of the system, the control system should also ensure stable operation of the system. In the process of designing the controller, the simplified system models will be used.

Ideally, a controller should decrease the rise, settling and peak times and decrease the overshoot. The controller that will be designed will have con-

stant gains, so a controller that works for both cases of coupling coefficient will be found.

Before starting the design of the control system, the system characteristics will be examined. For this, the approximated models of the system will be used. The system characteristics of the unregulated systems are shown in Table 6.1 and the step responses for the systems are shown in Figure 6.1.

	Overshoot	Rise time	Settling time
$H_{red,low}$	83.86%	$2.67 \cdot 10^{-4}$	0.017
$H_{red,high}$	48.52%	$1.36 \cdot 10^{-4}$	0.0019

Table 6.1: System characteristics of the step response of the systems.

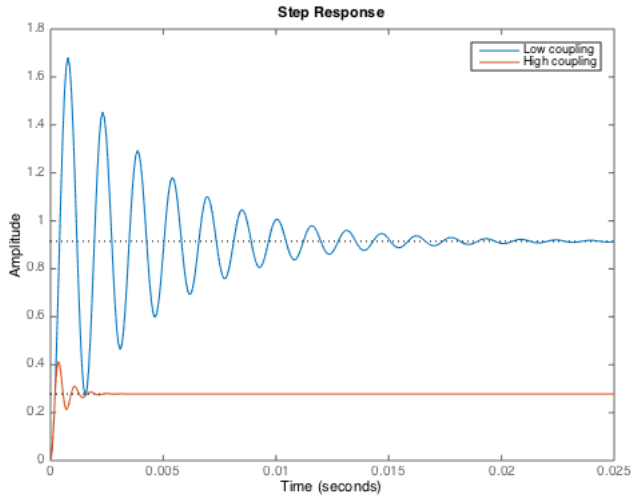

Figure 6.1: Open loop step responses of systems with low and high coupling.

The step responses shown in Figure 6.1 show that the systems of different coupling give very different open loop step responses. From Table 6.1 it

is easy to see that the systems have varying overshoot, rise and settling times, which must also be expected to see in a control system with constant controller gains.

Figure 6.2 shows the Bode plots of the two systems. An examination of the Bode plot and the step response plot leads to the following conclusions about the systems: For the system with low coupling coefficient the system bandwidth (frequency at which the magnitude of the frequency response drops 3 dB from its zero frequency value) is smaller than for the system with high coupling coefficient. A wider bandwidth indicates a shorter rise time for the transient response and by that a quicker response. This is shown in the step responses of the systems in Figure 6.1. Next, it can be observed from the Bode plot that the system with low coupling coefficient has a larger resonant peak than the system with high coupling coefficient. The resonant peak is the peak of the magnitude of the frequency response. The resonant peak of a system is related to the maximum overshoot of a system in the way that a large resonant peak leads to a large overshoot in the transient response. Table 6.1 shows that this is the case for the two systems investigated.

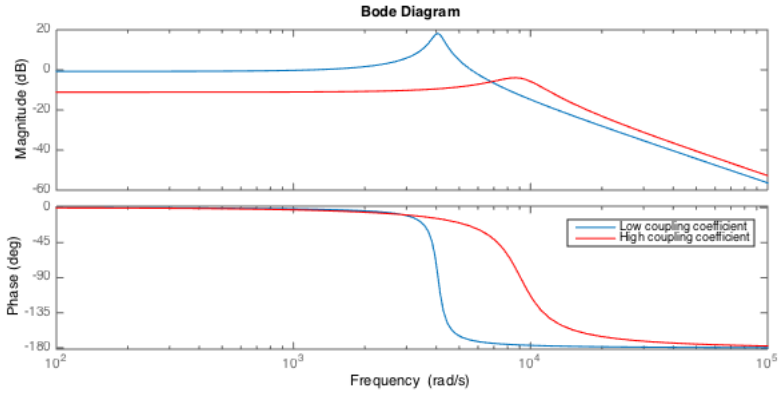

Figure 6.2: Bode plots of systems with low and high coupling.

From Table 6.1 and Figures 6.1 and 6.2 some observations can be made which will be the basis for the design of the control system. First of all, both systems have a very high overshoot. Secondly, it is clear the systems need integral control: When a step response with an amplitude of 1 is applied to the systems, none of them reach 1 as their steady state value. To eliminate this steady state error, it is necessary with integral control. Lastly, it is observed that both rise and settling times are low for both systems. In order to achieve good regulation of the systems, these short rise and settling times may be compromised in order to achieve a zero steady state error.

6.2 Haalman's Loop Shaping Method

Halman's loop shaping method is based on the ideal loop transfer function G_l. Choosing G_l to be the transfer function that gives the same settling time as the original simplified transfer functions and with no overshoot gives

$$G_{l,low} = \frac{1}{(0.0001s + 1) \cdot 0.004s} \tag{6.1}$$

and

$$G_{l,high} = \frac{1}{(0.0001s + 1) \cdot 0.0005s} \tag{6.2}$$

Using the formula presented in Chapter 4.4 to find the controller transfer function yields

$$G_{c,low} = \frac{G_{l,low}}{H_{red,low}} = \frac{s^2 + 455.9s + 1.659 \cdot 10^7}{6.07s^2 + 6.07 \cdot 10^4 s} \tag{6.3}$$

and

$$G_{c,high} = \frac{G_{l,high}}{H_{red,high}} = \frac{s^2 + 4064s + 8.238 \cdot 10^7}{1.145s^2 + 1.145 \cdot 10^4 s} \tag{6.4}$$

From looking at the controller transfer functions, it is clear that these controllers are not PID controllers. The controllers follow the formula $\frac{s^2+c_1 s+c_0}{d_2 s^2+d_1 s}$, in which the constants c_1, c_0, d_2, and d_1 vary depending on the coupling between the sending and receiving coils. This general formula can be represented in the form

$$\frac{s^2 + c_1 s + c_0}{s(d_2 s + d_1)} = \frac{s^2 + c_1 s + c_0}{s} \cdot \frac{1}{d_2 s + d_1} \tag{6.5}$$

The first part of the last expression is recognized as the Laplace transform of the PID controller with $K_p = c_1$, $K_i = c_0$ and $K_d = 1$. The control system using Haalman's loop shaping method for this system is therefore a PID controller in series with a filter given by $\frac{1}{d_2 s+d_1}$.

These controllers give the step responses as shown in Figure 6.3. The step responses show that the controllers give a good response to a step: In both cases the oscillations seen in the step responses of the unregulated systems are eliminated without compromising the settling times. The Bode plots for these cases are shown in Figure 6.4. From the plots it is observed that the resonant peak found in the frequency response of the unregulated systems is completely attenuated.

The next step is to investigate how the systems with high and low coupling coefficients react in a control loop controlled by the regulator designed for the opposite coupling coefficient case. In the case of regulating the system with low coupling coefficient with the regulator represented by $G_{c,high}$, the closed loop system response becomes unstable. The resulting step response plot of regulating both systems with the controller represented by $G_{c,low}$ is shown in Figure 6.5. The step response indicates that this controller works well for both systems, giving a minimum settling time of 15.4 ms and a

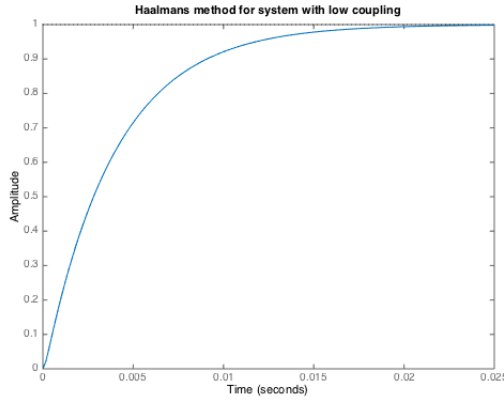

(a) Low coupling

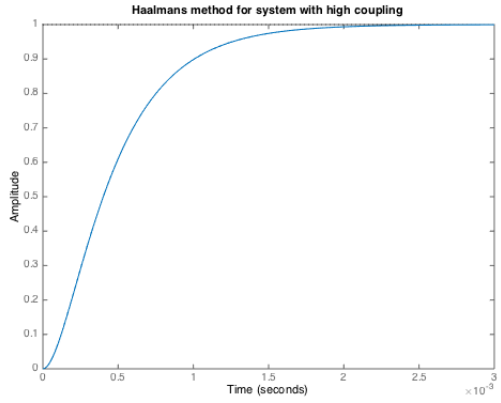

(b) High coupling

Figure 6.3: Plots showing step responses of systems with controllers found using Haalman's loop shaping method.

maximum settling time of 51.1 ms for low and high coupling, respectively. The Bode plots of the systems reveal that there is a peak in the magnitude

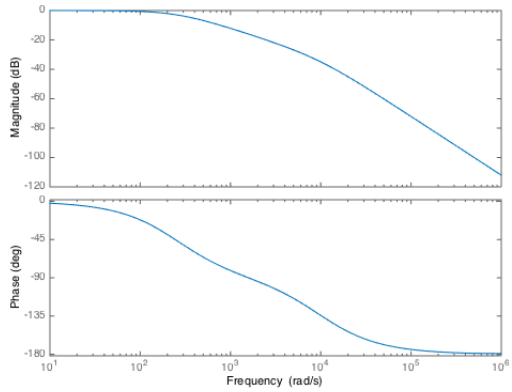

(a) Low coupling

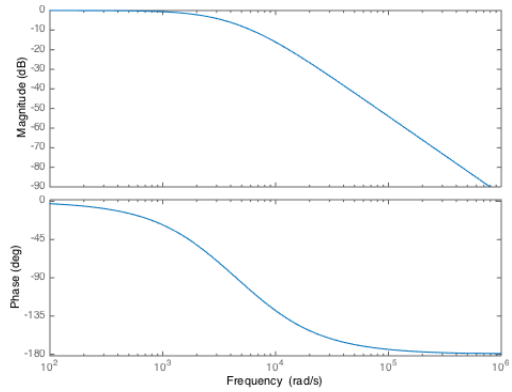

(b) High coupling

Figure 6.4: Bode plots for systems with controllers found using Haalman's loop shaping method.

and phase plots of the system with high coupling coefficient. This resonant peak is placed around the resonant frequency of this system. As the system

will operate around this frequency, this peak in both magnitude and phase is positive, as it will give a better functioning system around this frequency.

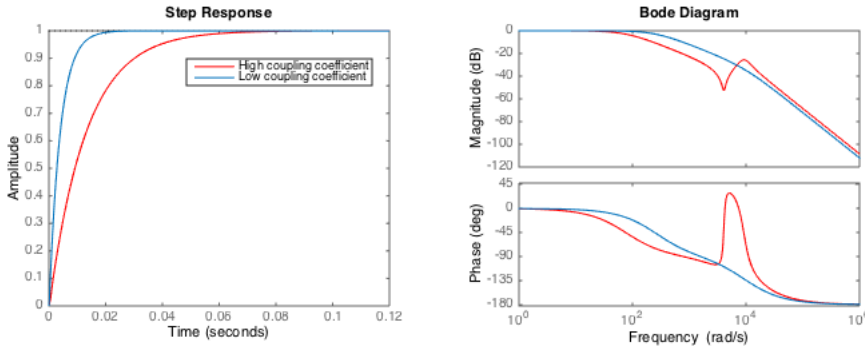

Figure 6.5: Step response and Bode plot of systems with both coupling coefficients regulated by $G_{c,low}$.

The chosen controller is now tested on the full transfer functions for the systems of high and low coupling coefficient. The results are shown in Figures 6.6 and 6.7. The Bode plots show that the controller works well on the full systems. The simplified and full transfer function plots match perfectly up to frequencies above resonance for both cases. At frequencies above this there is some deviation between the original and simplified models, but this is expected, as there was a deviation between these without the controller as well. For the step response plots, the full and simplified systems match perfectly.

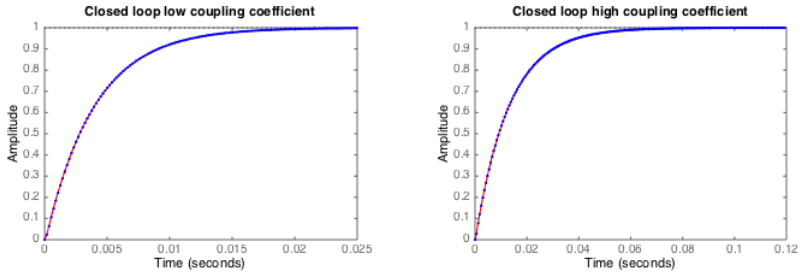

Figure 6.6: Step response plots of full and simplified systems with chosen controller. Red color indicates full system transfer function, blue dots indicate simplified transfer function.

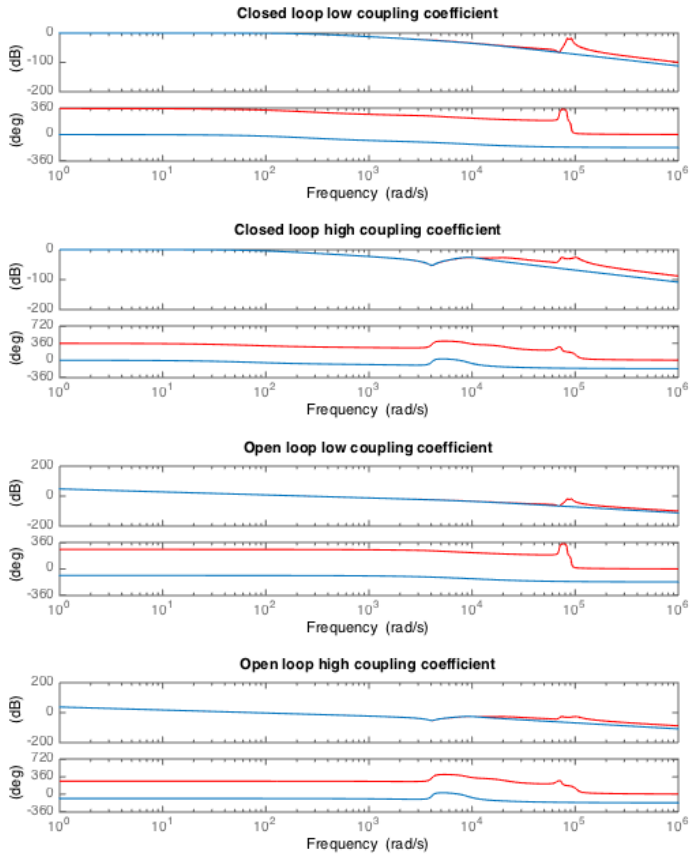

Figure 6.7: Bode plots of full and simplified systems with chosen controller. Red color indicates full system transfer function, blue color indicates simplified transfer function.

6.3 Experimental Tuning by Tuning Maps

Tuning maps will be used to design a controller for the IPT system. As a first step, a tuning map for a PI controller will be used in the tuning of the controller, and if it is seen as necessary, a tuning map for the derivative term will be added. The first tuning map will examine how the system responds to a controller with the controller parameters varying between 0.1, 1 and 10. The tuning map shown in Figure 6.8 shows the tuning map for the system with low coupling coefficient and K_p and K_i as indicated in the tuning map.

From the tuning map it is observed that the controller with a low value for the proportional gain gives the best response. In this case, the quickest response is achieved with the highest value for the integral term. A new tuning map is now made with values of K_p and K_i based on this result and shown in Figure 6.9. This tuning map shows that the closed loop response is quicker with $K_i = 50$, and rises smoother with the smallest value for K_p. Based on these results a purely integral controller is looked into.

Figure 6.10 shows the tuning map for an integral only controller with the gains as indicated in the figure for the system with low coupling coefficient. Increasing the integral gain decreases the rise time of the step response, but also causes the response to have more noise (A zoomed plot of this can be found in Appendix A.3). In order to get a response without noise, $K_i = 40$ is chosen as the integral gain for the controller. A new tuning map could be made to examine the response around this integral gain, but the analysis is stopped at this point.

Assuming that the tuning maps for the system with high coupling coefficient will result in the same conclusion regarding an integral only controller being a good choice, the analysis for the system with high coupling coefficient will start with the integral only controller. For the case of higher coupling coefficient it is found that the integral gain of the case with low coupling coefficient can be multiplied by a factor of ten and still give a stable and smooth response. However, a controller with this gain will not work on

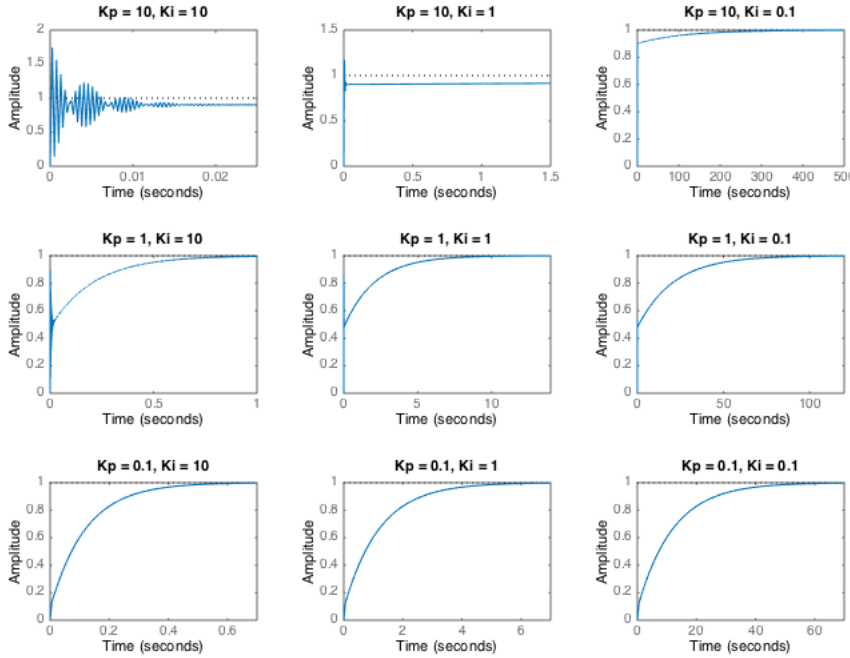

Figure 6.8: Tuning map for PI controller of system with low coupling coefficient.

the system with low coupling coefficient, as it has been discussed that the maximum gain wanted for that system is around $K_i = 40$. Therefore, the response of the two systems for different coupling will be examined with the controller found for $H_{red,low}$.

The tuning map of Figure 6.11 shows the response of the two systems with $K_i = 40$. For the system with high coupling coefficient, the response is quite slow with a settling time of 0.35 seconds. Considering that the sending and receiving coils might have much movement relative to each other, it

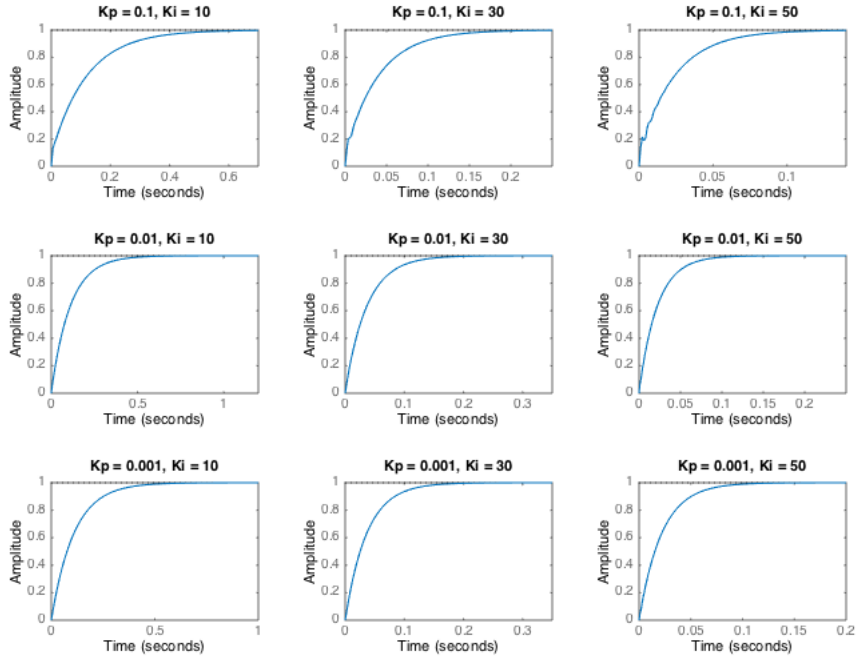

Figure 6.9: Tuning map for PI controller of system with low coupling coefficient.

is attempted to decrease the settling time. Two other integral gains are tested for the systems: $K_i = 90$ and $K_i = 140$, varying the integral gain with 50 for each step. Figure 6.11 shows that with the controller with an integral gain of 140, the settling time is decreased to 0.1 s for the system with high coupling coefficient.

Figure 6.12 shows the Bode plots for the open and closed loop systems with high and low coupling coefficients and the proposed controller. It is observed that the resonant peak that was completely attenuated when

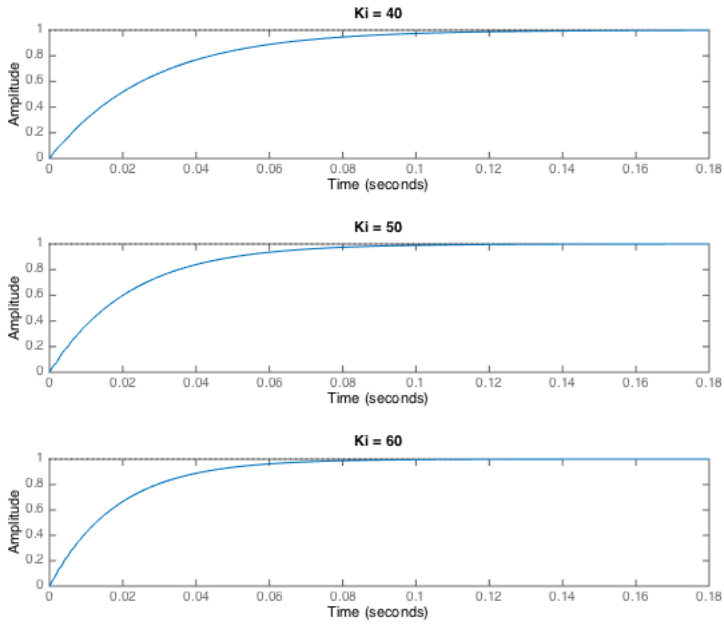

Figure 6.10: Tuning map for I controller of system with low coupling coefficient.

controlling the systems with the regulator found in the previous section, are present when using the integral only controller, although greatly attenuated compared with the unregulated system. However, the resonant peak in the Bode plot in this case gives a better performance for the system around the resonance frequency as the resonant peak leads to the output of the system being closer to the input in magnitude.

The response of the full systems regulated by this controller is now looked into. Figures 6.13 and 6.14 show the Bode and step response plots of the systems, respectively. These plots show the responses for both the full

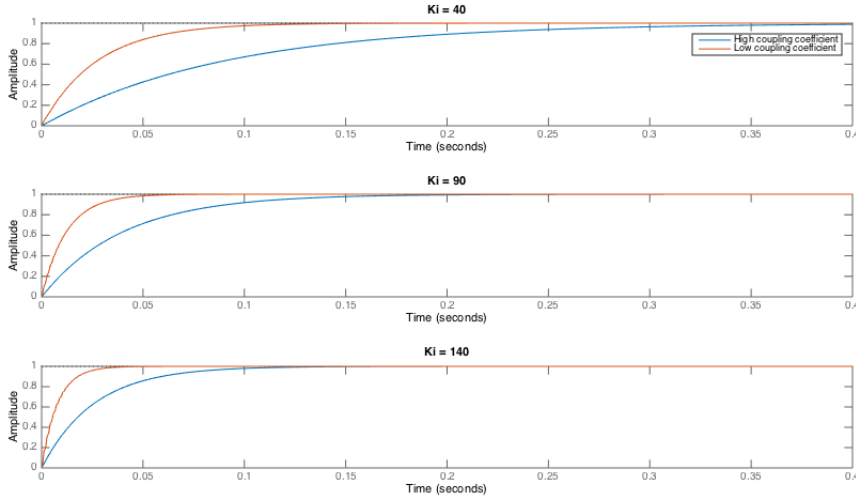

Figure 6.11: Tuning map for I controller of system with low and high coupling coefficients.

transfer functions and their simplifications.

The Bode plots shows that the controller works well for frequencies up to the resonant frequencies of the systems. At frequencies above the resonant frequency, the controller leads to good performance. The step responses also show that the controller regulates the full systems as well as it does the approximated ones.

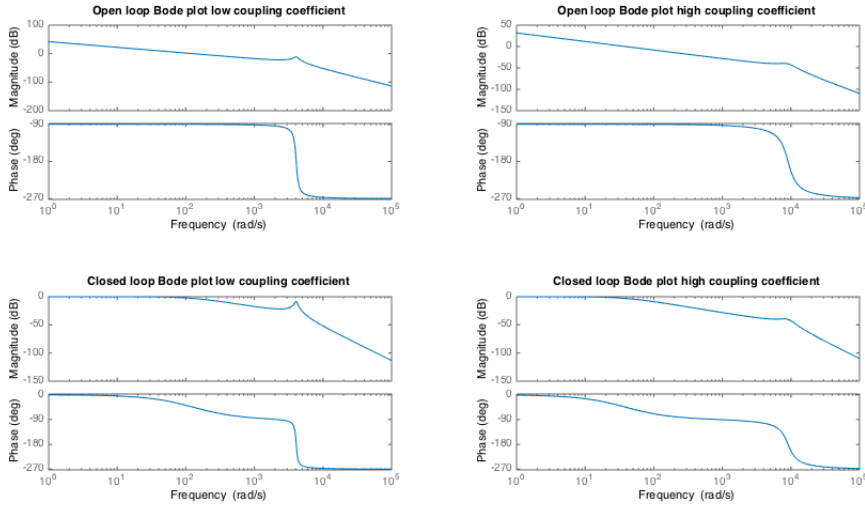

Figure 6.12: Open and closed loop Bode plots for systems with controller $K_i = 140$.

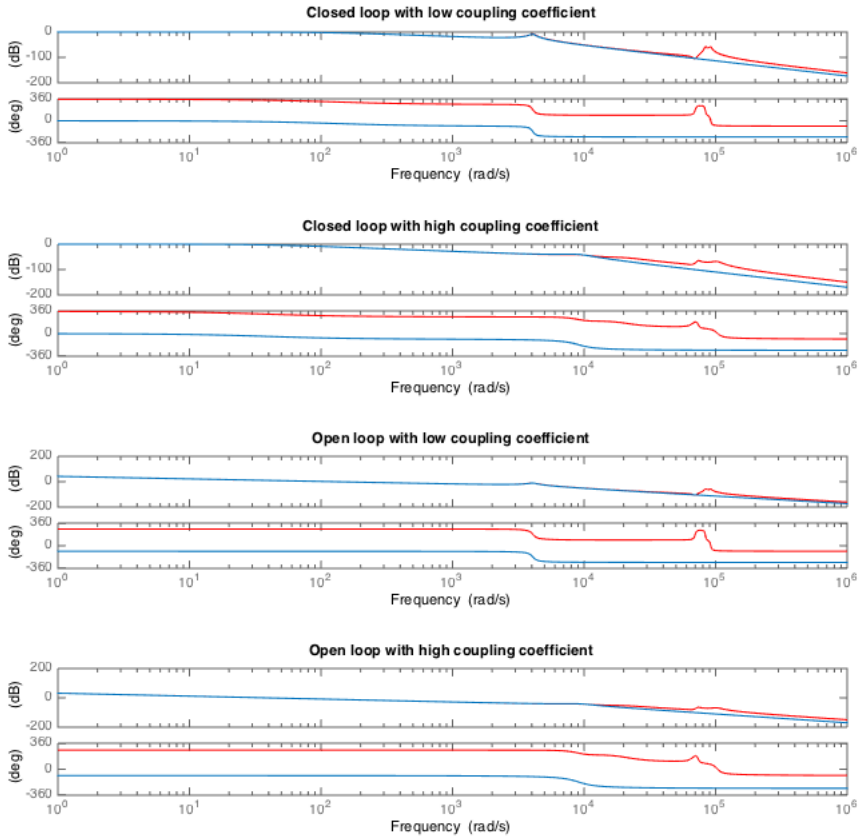

Figure 6.13: Bode plots for systems with controller $K_i = 140$. Red color indicates full transfer function, blue color indicates simplified transfer function.

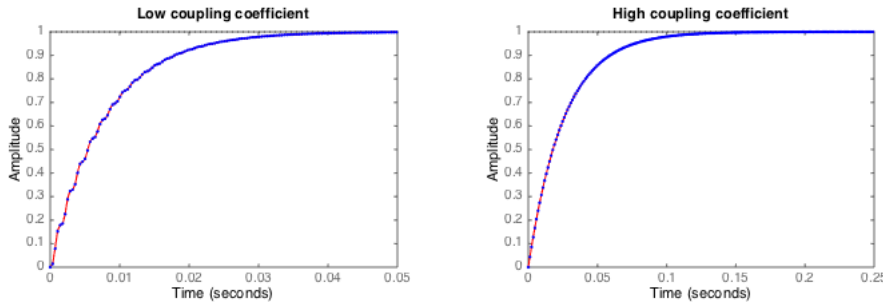

Figure 6.14: Step response plots for systems with controller $K_i = 140$. Red color indicates full transfer function, blue dots indicate simplified transfer function.

Chapter 7

Results and Discussion

Looking at the step responses of Figure 7.1 shows that the systems regulated by the controller found using Haalman's loop shaping method (from this point and on referred to as G_c) give a quicker response for both the system with high and low coupling. Controlling the system with low coupling with the integral-only controller G_i yields a step response with some vibration during the rise of the response. The choice of this value for the integral gain was discussed in the previous chapter and this behaviour of the step response is, based on that discussion, accepted.

The amplitude-phase-frequency diagrams for the systems with low and high coupling coefficients regulated by each of the proposed controllers is shown in Figure 7.2. In the Bode plots, the controller found using Haalman's loop shaping method is represented by blue color, and the controller found using tuning maps is represented by red color. The plots show that for operation around the resonant frequency the systems regulated by the integral-only controller give the best response, but at frequencies above this, the controller represented by its transfer function G_c gives the best response, both in terms of magnitude and phase shift.

From the open loop Bode plots, the gain and phase margins for the system

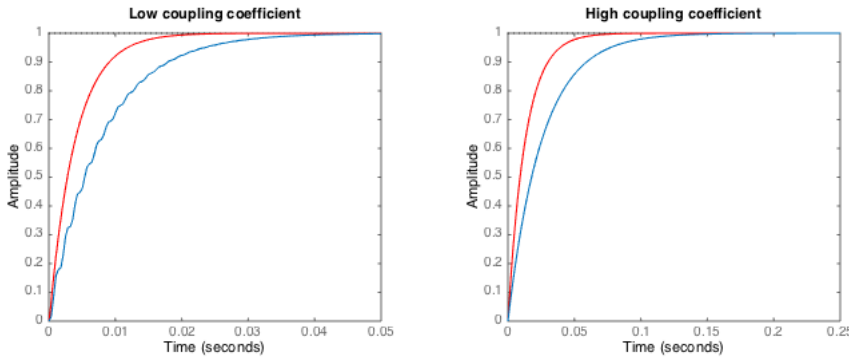

Figure 7.1: Step response plots for systems with both proposed controllers. Red color indicates system controlled by G_c, blue indicates system controlled by integral only controller.

can be found as indicated in Table 7.1. As seen, the phase margin is more or less the same for all the open loop systems. The gain margins, however, vary more with the two controllers. When using G_i to control the system with low coupling coefficient, the gain margin is Gm = 10.3 dB. This is the lowest gain margin for any of the cases investigated, but it is within the margins of stability. All the systems are closed loop stable.

	G_c	G_i
Low k	Gm = 22.4 dB, Pm = 88.9^o	Gm = 10.3 dB, Pm = 90^o
High k	Gm = 30.8 dB, Pm = 89.7^o	Gm = 52.1 dB, Pm = 90^o

Table 7.1: Gain (Gm) and phase (Pm) margins of systems with different controllers.

The two controllers are represented in the Laplace domain as

$$G_c = \frac{s^2 + 455.9s + 1.659 \cdot 10^7}{s} \cdot \frac{1}{6.07s + 6.06 \cdot 10^4} \tag{7.1}$$

and

$$G_i = \frac{140}{s} \tag{7.2}$$

Here, G_c is the controller found using Haalman's loop shaping method and G_i is the integral only controller found by experimental tuning by the help of tuning maps. G_c is a PID controller in series with a first order filter. G_i, on the other hand, is purely an integral controller. This controller is a lot simpler than the controller represented by G_c, and easier to implement, but, as shown, results in a system with slower response.

The two methods used for the controller design, Halman's loop shaping method and experimental tuning using tuning maps, are, of course, not guaranteed to lead to the best controller for the systems. In the process of using Halman's loop shaping method, an optimal loop function was chosen based on the wanted rise time of the response. If other criteria were included in the design of the ideal loop function, the controller design would also be different. When using tuning maps, it is up to the designer to choose when the system's response if satisfactory. It would be possible to make the system response quicker using an integral-only controller, but as the system response was found to be satisfactory with an integral gain of 140, the analysis was stopped at that value. The tuning maps method used in Chapter 6 was based on the system's response to a step input, but tuning maps can also be used with frequency response plots. This would most likely lead to a different result for the controller.

The system used in the analysis when finding a controller is simplified in many steps: The IPT system was first simplified to an equivalent diagram which was used to find a mathematical model of the system. In the derivation of this mathematical model, several assumptions and simplifications were made, as operation around the resonant frequency and the assumption of a time-invariant load. The resulting transfer function was again simplified to get a representation of the system more suitable for the analysis of this thesis. Lastly, all disturbances in the system and feedback control

loop were ignored. When looking at the results, the fact that all of these assumptions and simplifications have been made, needs to be taken into consideration. The results can therefore be used as an indication to what the control system can be like, but a less simplified and more detailed model should be derived and used as a design base.

The validity of the mathematical model should be checked through a simulation or laboratory model. If this investigation leads to big differences between the response of the mathematical model and the simulation/laboratory experiment, the mathematical model of the system needs to be reevaluated, and with that also the designed controllers.

The two control systems proposed are simple control systems, both with only one feedback loop. The responses of the systems can be further changed to meet stricter design restrictions, if that is wanted, by designing a more complex control system. However, the two proposed control systems result in stable systems with quick response for both low and high coupling coefficients.

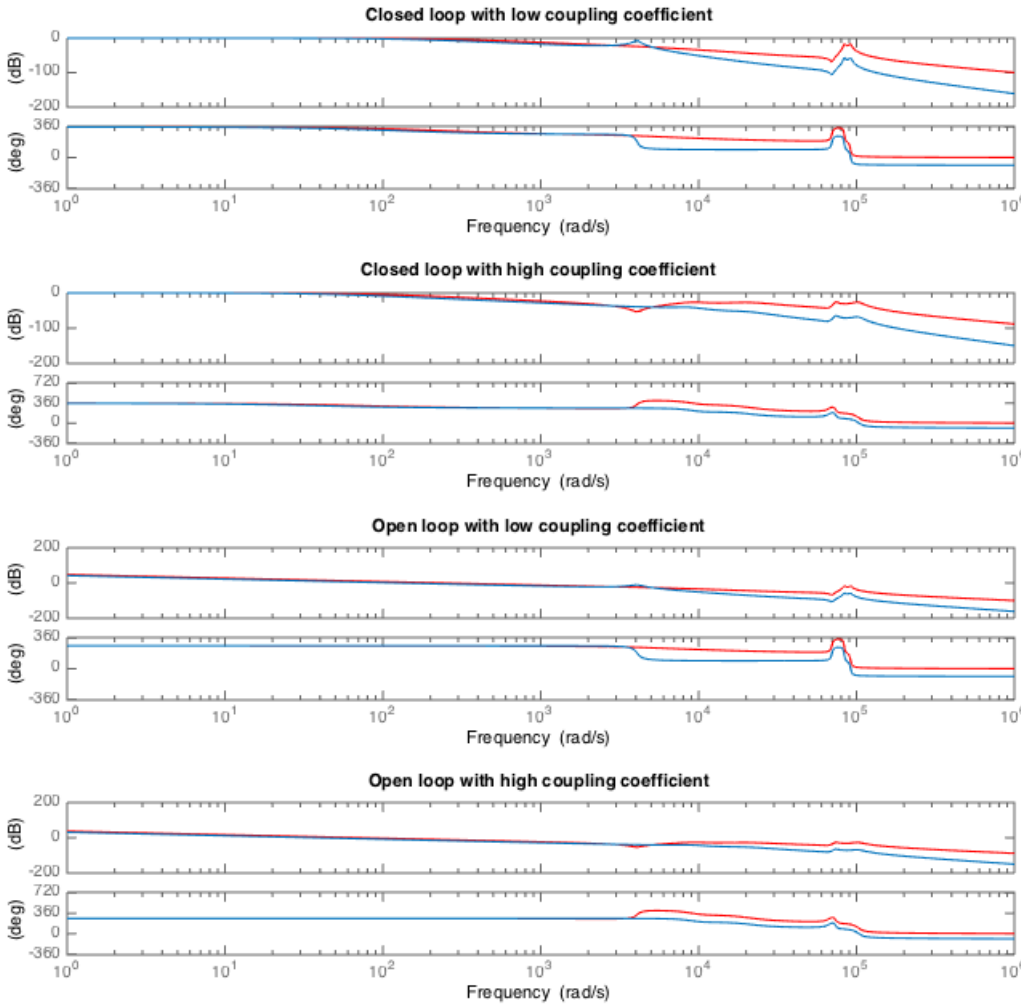

Figure 7.2: Bode plots for systems with both proposed controllers. Red color indicates system controlled by G_c, blue indicates system controlled by integral only controller.

Chapter 8

Conclusion

Two methods for control design have been used to design two independent controllers with constant gains for a system for inductive charging of electric ferries: (1) Haalman's loop shaping method, and (2) experimental tuning with the use of tuning maps. The system has been simplified and represented mathematically in the Laplace domain as $H(s) = \frac{a_0}{s^2+b_1 s+b_0}$ where a_0, b_1 and b_0 depend on the coupling of the system.

The two designed controllers are represented by their Laplace transforms as $G_c(s)$ and $G_i(s)$. When comparing the system response to the two controllers, their step and frequency responses were looked into. The controller represented by G_c gave a system with quicker response to a step change in the input. When it comes to the frequency response, the integral-only controller represented by G_i gave a better response around the resonant frequency. In addition, this controller is a lot simpler and thereby also easier to implement. On basis of this, the integral-only controller is proposed as the best controller for the system. This controller is given by $G_i = \frac{140}{s}$.

Both control designs are designed based on and tested on a mathematical model of a simplified system for inductive power transfer. The validity of the control system on the full system is therefore limited and needs to be

investigated in a laboratory or a simulation tool. If this investigation leads to big differences between the response of the mathematical model and the simulation/laboratory experiment, the mathematical model of the system needs to be reevaluated. Otherwise, the found controller can be used either as it is or as a starting point for design of a more complex control system.

Chapter 9

Further Work

The integral time performance criteria can be used to find the optimal controller gains, but this requires a good understanding of mathematics and the Laplace and time domains. The formulas presented in Chapter 4 can be used to find the optimal controller gains.

Further, an IPT system should be simulated and the controller performance as well as the validity of the mathematical model should be checked using the simulation model. After this, a laboratory set up can also be used to validate the system performance with the chosen controller.

Bibliography

[1] US Department of Energy, *The history of the Electric Car*, September 15th, 2014, http://energy.gov/articles/history-electric-car.

[2] Covic, G. A., Boys, J. T., *Inductive Power Transfer*, Proceedings of the IEEE, Vol. 101, June 2013, pp. 1276-1289.

[3] RamRakhyani, A. K., Mirabbasi, S., Chiao, M., *Design and Optimization of Resonance-Based Efficient Wireless Power Delivery Systems for Biomedical Implants*, IEEE Transactions on Biomedical Circuits and Systems, Vol. 5, No. 1, February 2011, pp. 48-63.

[4] Wang, G., Liu, W., Sivaprakasam, M., Kendir, G. A., *Design and Analysis of an Adaptive Transcutaneous Power Telemetry for Biomedical Implants*, IEEE Transactions on Circuits and Systems, Vol 52, October 2005, pp. 2109-2117.

[5] Thirugnanam, K., Ezhil Reena Joy, T.P., Singh, M., Kumar, P., *Modeling and Control of Contactless Based Smart Charging Station in V2G Scenario*, IEEE Transactions on Smart Grid, Vol. 5, No. 1, January 2014.

[6] Patrick, S. *Nikola Tesla - Imagination and the Man That Invented the 20th Century.* 2013

[7] Schuder, J. C., Gold, J. H., Stephenson, H. E., *An inductively coupled RF system for the transmission of 1 kW of power through the skin*,

IEEE Transactions on Bio-Medical Engineering, vol. 18, no. 4, 1971, pp. 265–273.

[8] Cogan, R., *The Electric Experience*, Popular Science, November 1996, pp. 81-84.

[9] Austin, M., *Electrified Public Transportations Promises Residual Value*, http://electricvehicle.ieee.org/2015/01/08/electrified-public-transportations-promises-residual-value/

[10] Valle, M., *Alt du trenger å vite om trådløs lading*, Teknisk Ukeblad, October 2013.

[11] Jurjevich, M., *Large Scale, Commercial Wireless Inductive Power Transfer (WIPT) for Fixed Route Bus Rapid Transportation* http://electricvehicle.ieee.org/2014/09/02/large-scale-commercial-wireless-inductive-power-transfer-wipt-fixed-route-bus-rapid-transportation/

[12] Mohan, N., Undeland, T., Robbins, W. *Power Electronics*. 3rd edition. USA: John Wiley & Sons, Inc.; 2003.

[13] Madawala, U., Neath, M., Thrimawithana, D., *A Power-Frequency Controller for Bidirectional Inductive Power Transfer System*. IEEE Transactions on Industrial Electronics, Vol. 60, No. 1, January 2013.

[14] Thrimawithana, D. J., Madawala, U. K., *A Primary Side controller for Inductive Power Transfer Systems*. IEEE International Conference on Industrial Technology (ICIT), 2010, pp. 661-666.

[15] Si, P., Hu, A. P., Hsu, J. W., Chiang M., Wang, Y., Malpas, S., Budgett, D., *Wireless Power Supply for Implantable Biomedical Device Based on Primary Voltage Regulation*. Second IEEE Conference on Industrial Electronics and Applications, 2007, pp. 235-239.

[16] Stielau, O. H., Covic, G.A., *Design of Loosely Coupled Inductive Power Transfer System*, PowerCon 2000 International Conference on Power System Technology, 2000, pp. 85-90.

[17] Hassan, F.A., *Power Efficient Battery Charger by Using Constant Current/Constant Voltage Controller.* Circuits and Systems, 2012, 3, pp. 180-186.

[18] Astrom, K. J., Hagglund, T. H., *New Tuning Methods for PID Controllers*, Proceedings of the 3rd European Control Conference, 1995.

[19] Balchen, J. G., Andresen, T., Foss, B. A. *Reguleringsteknikk.* 5th edition. Trondheim, Norway: Institutt for teknisk kybernetikk, NTNU; 2003.

[20] Bennet, S., *Development of the PID Controller*, IEEE Control Systems, 1993.

[21] Shakhrokhi, M., Zomorrodi, A., *Comparison of PID Controller Tuning Methods*,

[22] Nilsson, J. W., Riedel, S. A. *Electric Circuits.* 8th edition. New Jersey, USA: Pearson Education Inc.; 2008.

[23] Boz, A. F., Sari, Y., *Generalized Optimal Controller Design for all Pole Systems Using Standard Forms.* Scientific Research and Essay Vol. 4, March 2009, pp. 167-174.

[24] Åström, K., Hägglund, K. *PID Controllers: Theory, Design, and Tuning.* 2nd edition. USA: Instrument Society of America; 1995.

[25] Huang, Ch., Boys, J.T., Covic, G.A., Ren, S., *LCL Pick-up Circulating Current Controller for Inductive Power Transfer System*, Energy Conversion Congress and Exposition (ECCE), 2010 IEEE, September 2010, pp. 640-646.

[26] Guidi, G. *Project memo about control of IPT systems.* 2014, pp. 41-56.

[27] Chapman, S. J. *Electric machinery fundamentals.* 5th edition. USA: Mc Graw Hill; 2012.

[28] Boz, A. F., Sari, Y., *Generalized optimal controller design for all pole systems using standard forms*, Scientific Research and Essay Vol.4 (3), March, 2009, pp. 167-174.

Appendix A

Appendices

A.1 Derivation of input impedance for SS compensation configuration

$$-V_{send}+I_{send}\left(R_{eq1}+sL_1+\frac{1}{sC_1}\right)-sMI_{pick}=0,\quad R_{eq1}=R_1+R_{L_1}$$

$$I_{pick}\left(R_L+R_{eq2}+sL_2+\frac{1}{sC_2}\right)-sMI_{send}=0,\quad R_{eq2}=R_2+R_{L_2}$$

$$I_{pick}(s)=\frac{sMI_{send}(s)}{R_L+R_{eq2}+sL_2+\frac{s}{C_2}}$$

$$-V_{send}+I_{send}(s)\left(R_{eq1}+sL_1+\frac{s}{C_1}\right)-sM\frac{(sM)^2\,I_{send}(s)}{R_L+R_{eq2}+sL_2+\frac{s}{C_2}}=0$$

$$Z_{send,SS}=\frac{V_{send}}{I_{send}}$$

$$Z_{send,SS}=R_{eq1}+sL_1+\frac{s}{C_1}-sM\frac{sM}{R_L+R_{eq2}+sL_2+\frac{s}{C_2}}$$

$$s=j\omega$$

$$Z_{send,SS}=R_{eq1}+j\left(\omega L_1-\frac{1}{\omega C_1}\right)+\frac{\omega^2M^2}{R_L+R_{eq2}+j\left(\omega L_2-\frac{1}{\omega C_2}\right)}$$

$$Z_{send,SS}=R_{eq1}+j\left(\omega L_1-\frac{1}{\omega C_1}\right)+\frac{\omega^2M^2\left[R_L+R_{eq2}-j\left(\omega L_2-\frac{1}{\omega C_2}\right)\right]}{(R_L+R_{eq2})^2+\left(\omega L_2-\frac{1}{\omega C_2}\right)^2}$$

$$\mathrm{Re}\left\{Z_{send,SS}\right\}=R_{eq1}+\frac{\omega^2M^2\,(R_L+R_{eq2})}{(R_L+R_{eq2})^2+\left(\omega L_2-\frac{1}{\omega C_2}\right)^2}$$

$$\mathrm{Im}\left\{Z_{send,SS}\right\}=\left(\omega L_1-\frac{1}{\omega C_1}\right)-\frac{\omega^2M^2\left(\omega L_2-\frac{1}{\omega C_2}\right)}{(R_L+R_{eq2})^2+\left(\omega L_2-\frac{1}{\omega C_2}\right)^2} \tag{A.1}$$

A.2 MatLab Code

```
% Script used to find the simplified model of the system with low
% coupling.

% System model
%----------------------------------------------------------------------
P = 10^6;

Vs = 1000;

Vp = 1000;
1
L1 = 60.6*10^(-6);
L2 = 60.6*10^(-6);

M1 = 11.3*10^(-6); %low k

C1 = 8.7*10^(-6);
C2 = 8.7*10^(-6);

R1 = 5.6*10^(-3);
R2 = 5.6*10^(-3);
RL = 10;

f1 = 6.93*10^(3);

Ls = L1 - (((M1)^2)/(L2));

A = [-R1/Ls 2*pi*f1 ((M1)*(R2 + (Vp/Vs)*2*pi*f1*M1))/(Ls*L2) 0 -1/(Ls)
                                                        0 M1/(Ls*L2) 0;
     -2*pi*f1 -R1/Ls 0 (M1*R2)/(Ls*L2) 0 -1/(Ls) 0 M1/(Ls*L2);
     (M1*R1)/(Ls*L1) 0 -(R2 + (Vp/Vs)*2*pi*f1*M1)/(Ls) 2*pi*f1 M1/(Ls*L1)
                                                          0 -1/(Ls) 0;
     0 (M1*R1)/(Ls*L1) -2*pi*f1 -(R2)/(Ls) 0 M1/(Ls*L1) 0 -1/(Ls);
     1/(C1) 0 0 0 0 2*pi*f1 0 0;
     0 1/(C1) 0 0 -2*pi*f1 0 0 0;
     0 0 1/(C1) 0 0 0 0  2*pi*f1;
     0 0 0 1/(C1) 0 0 -2*pi*f1 0
```

```
     ];

B = [1/(Ls) ;
     0 ;
     -M1/(Ls*L2) ;
     0;
     0;
     0;
     0;
     0
     ];

C = [0 0 0 -(sqrt(2)/(pi)) 0 0 0 0;];

E = [0 0 0 0 0 0 0 0];

D = 0;

syscv6 = ss(A,B,C,D);

s = tf('s');

h = tf(syscv6);

%Simplification
%------------------------------------------------------------------------

c = pole(h);

hredlow1 = 1/((s-c(7))*(s-c(8)));

hredlow = (dcgain(h)/dcgain(hredlow1))*hredlow1;
```

```
%Script used to find the simplified model of the system with high
%coupling.

%System model
%------------------------------------------------------------------------

P = 10^6;

Vs = 1000;

Vp = 1000;

L1 = 68.1*10^(-6);
L2 = 68.1*10^(-6);

M1 = 39.4*10^(-6); %high k

C1 = 8.7*10^(-6);
C2 = 8.7*10^(-6);

R1 = 5.6*10^(-3);
R2 = 5.6*10^(-3);
RL = 10;

f1 = 6.54*10^(3);

Ls = L1 - (((M1)^2)/(L2));



A = [-R1/Ls 2*pi*f1 ((M1)*(R2 + (Vp/Vs)*2*pi*f1*M1))/(Ls*L2) 0
                                                  -1/(Ls) 0 M1/(Ls*L2) 0;
     -2*pi*f1 -R1/Ls 0 (M1*R2)/(Ls*L2) 0 -1/(Ls) 0 M1/(Ls*L2);
     (M1*R1)/(Ls*L1) 0 -(R1 + (Vp/Vs)*2*pi*f1*M1)/(Ls) 2*pi*f1
                                                  M1/(Ls*L2) 0 -1/(Ls) 0;
     0 (M1*R1)/(Ls*L1) -2*pi*f1 -(R2)/(Ls) 0 M1/(Ls*L2) 0 -1/(Ls);
     1/(C1) 0 0 0 0 2*pi*f1 0 0;
     0 1/(C1) 0 0 -2*pi*f1 0 0 0;
     0 0 1/(C1) 0 0 0 0  2*pi*f1;
     0 0 0 1/(C1) 0 0 -2*pi*f1 0
```

```
     ];

B = [1/(Ls) ;
     0 ;
     -M1/(Ls*L2) ;
     0;
     0;
     0;
     0;
     0
     ];

C = [0 0 0 -(sqrt(2)/(pi)) 0 0 0 0;];

E = [0 0 0 0 0 0 0 0];

D = 0;

syscv6 = ss(A,B,C,D);

s = tf('s');

h = tf(ss(A,B,C,D));

%Simplification
%-------------------------------------------------------------------------

c = pole(h);

hredhigh1 = 1/((s-c(7))*(s-c(8)));

hredhigh = (dcgain(h)/dcgain(hredhigh1))*hredhigh1;
```

A.3 Zoomed Tuning Map

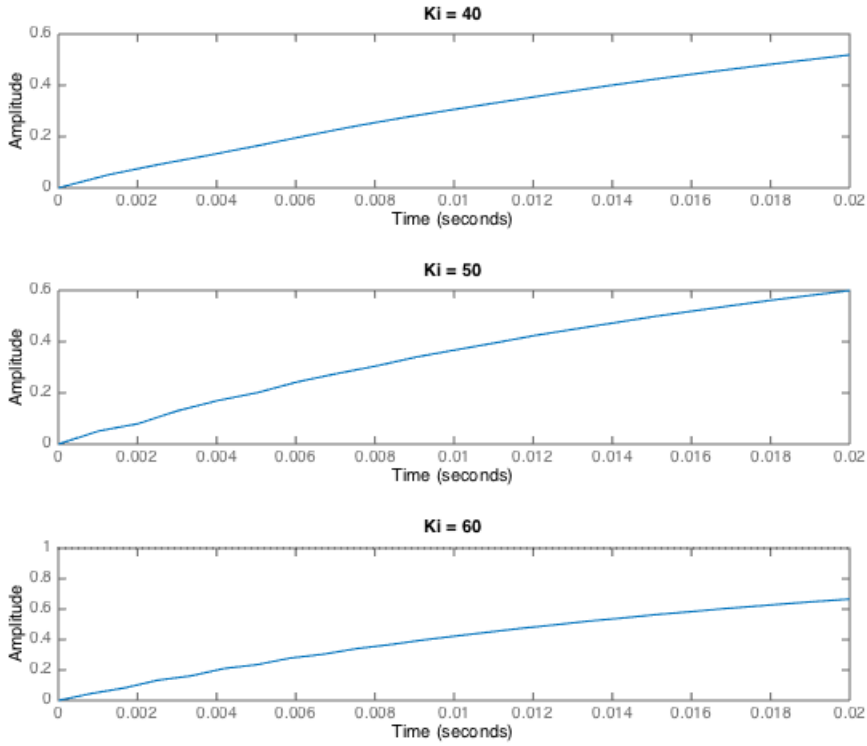

Figure A.1: Zoomed tuning map for I-only controller.